Journal of Structural Geology 31 (2009) 403–420

Contents lists available at ScienceDirect

Journal of Structural Geology

journal homepage: www.elsevier.com/locate/jsg

Extensional fault cores in micritic carbonate – Case studies from the Gulf of Corinth, Greece

Eivind Bastesen [a,b,*], Alvar Braathen [b,c], Henning Nøttveit [a], Roy H. Gabrielsen [a,d], Tore Skar [a,e]

[a] Centre for Integrated Petroleum Research, University of Bergen, 5020 Bergen, Norway
[b] Department of Earth Science, University of Bergen, 5020 Bergen, Norway
[c] University Centre in Svalbard, 9171 Longyearbyen, Norway
[d] Department of Geosciences, University of Oslo, Box 1047 Blindern, 0316 Oslo, Norway
[e] StatoilHydro, Stavanger, Norway

ARTICLE INFO

Article history:
Received 15 May 2008
Received in revised form
10 December 2008
Accepted 11 January 2009
Available online 20 January 2009

Keywords:
Extensional faults
Micritic carbonate
Fault core
Undulating slip surface
Lenses
Fault rock

ABSTRACT

The major Pisia and Doumena faults of the Corinth Rift, Greece, are both hosted by micritic carbonate rock. Their common fault elements are principal slip surfaces, layers of fault rocks, fault rock and host rock lenses, corrugations, and smaller shear and tension fractures. Along planar fault segments, a corrugated slip surface with an associated thin fault rock layer is formed. Well-developed down-dip corrugations indicate movement along the same surface over many fault increments. Bends/jogs in the faults are sites of complex structural relations, hosting frequent lenses, more porous fault rocks, and dense networks of fractures. Major jogs in the slip surfaces have both strike and dip-oriented undulating curvature that are associated with higher order fracture networks as well as frequent lenses.

Fault core lens shapes of the Doumena fault show relationship of length vs. width of 3/2. Similarly, principal slip surfaces of the two faults show undulations with aspect ratios of amplitude vs. wavelength (1:19 and 1:14) in strike-direction, despite a prominent difference in down-dip geometry.

The intrinsic deformation in fault cores of micritic carbonate supports a model in which fluids entered the core by damage zone fractures that are linked to the principal slip surface. Flow along the fault core was controlled by the fracture system of lenses, and thereby lens connectivity, but may have been hampered by flow-retarding fault rocks. The flow potential is especially well developed in fault bends and breached relays due to frequent lenses and well-developed fracture networks.

1. Introduction

The internal geometry and distribution of fractures, fault rocks and zones of mineralization may have strong influence on fluid flow (e.g. Caine et al., 1996; Childs et al., 1997; Evans et al., 1997; Cello et al., 2003; Micarelli et al., 2003; Geraud et al., 2006; De Paola et al., 2007, 2008). These parameters are therefore of particular importance in the construction of numerical fluid flow models of fault zones (Sverdrup et al., 2001; Bonson et al., 2007; Fredman et al., 2007). A well-developed fault encompasses a footwall and a hanging-wall damage zone with an enhanced fracture frequency and a fault core, where most of the displacement is accommodated (e.g. Chester and Logan, 1986; Chester et al., 1993; Caine et al., 1996). Intrinsically, the fault core commonly includes slip surfaces separating tabular layers or lenses of fault rocks or country rock deformed to different degree (Gibbs, 1983; Woodcock and Fisher, 1986; Childs et al., 1996b; Childs et al., 1997; Gabrielsen and Clausen, 2001; Clausen et al., 2003; Lindanger et al., 2007).

Generalized models predict fault cores to be either fluid conductors or fluid flow obstacles, both along and across the fault zone. Communication across a fault zone may be enhanced where lenses of highly permeable rock are juxtaposed (Childs et al., 1997; Knipe et al., 1998; Gabrielsen and Clausen, 2001) where communication occurs through open fractures (Cello et al., 2001; Geraud et al., 2006), or where permeable breccia units are abundant (Tarasewicz et al., 2005; Chambon et al., 2006).

In this paper we investigate the complex architecture of fault cores in large extensional faults, with special focus on geometrical, spatial and statistical trends of slip surfaces, fractures, lenses and fault rocks. This issue is addressed through the analysis of two well-exposed extensional faults near Corinth, Greece, the Doumena and

* Corresponding author at: Department of Earth Science, University of Bergen, 5020 Bergen, Norway. Tel.: +47 99230248.
E-mail address: eivind.bastesen@cipr.uib.no (E. Bastesen).

0191-8141/$ – see front matter © 2009 Elsevier Ltd. All rights reserved.
doi:10.1016/j.jsg.2009.01.005

Pisia faults of the Corinth Rift. These are situated in Mesozoic carbonates and have a hanging-wall section of Pliocene syn-tectonic clastics. Exposures of the master fault planes (principal slip surfaces) of the two faults are more than 100 × 100 m in extent, and are also in places excavated by ravines. Such outcrops offer an unusual good opportunity for detailed study of fault surface morphologies as well as the structural geometry of fractures, fault lenses and fault rock units. For both faults, we have undertaken systematic structural and morphological mapping in fault-parallel and fault-perpendicular sections of the slip surface, and by that documenting that the two faults are strikingly different: The Doumena fault is dominated by fault lenses of protolith rock and fault rocks, each delineated by high-strain zones, and the principal slip surface is marked by both strike- and dip-parallel corrugation lines. In contrast, few fault lenses are preserved in the core of the Pisia Fault and its principal slip surface is characterized by down-dip corrugations and layers of fine-grained fault rocks and flowstone.

2. Geological framework

The two studied faults are located at the southern margin of the active Gulf of Corinth, Greece, which presently experiences crustal stretching in a 110 km long and 30 km wide region. The extension rate of 1.5 cm/year (Fig. 1) (e.g. Sorel, 2000; Moretti et al., 2003).

The Doumena fault (Causse et al., 2004; Chambon et al., 2006) is situated in the northern part of Peloponnesus, near the village of Kalavrita. This fault is considered inactive (Flotté and Sorel, 2001). The Pisia fault (Stewart and Hancock, 1991; Roberts and Stewart, 1994) is located near the eastern end of the rift, near the town of Loutraki. In February 1981 the Pisia fault was reactivated in a 6.7 Magnitude earthquake, causing nearly 2 m of ground surface separation at the study site (e.g. Jackson et al., 1982; Hubert et al., 1996; Roberts and Koukouvelas, 1996; Kokkalas and Koukouvelas, 2005).

Regional extensional Corinth rifting was initiated ca. 1 Myr ago (see summary in Moretti et al., 2003) as a consequence of back-arc spreading in the foreland of the Hellenic Trench (Le-Pichon and Angelier, 1979; Doutsos and Kokkalas, 2001; Koukouvelas et al., 2005; Leeder et al., 2008). Rifting triggered activity on several main fault segments that strike WNW-ESE, revealing present displacement vectors oriented N-S (Jackson and McKenzie, 1999; Morewood and Roberts, 2001). The rift system is characterized by asymmetric opening rates, varying from 1.5 cm/y in the west to 0.5 cm/y in the east (Briole et al., 2000; Goldsworthy et al., 2002; Moretti et al., 2003). The overall rift geometry is that of an asymmetric half graben, developing above a north-dipping detachment fault (Doutsos and Poulimenos, 1992; Armijo et al., 1996; Moretti et al., 2003). Main faulting is found along the southern flank of the rift, which is characterized by several large extensional fault blocks, while the northern flank is built up of smaller fault blocks associated with a regional rollover anticline (Sorel, 2000). The southern rift flank uplift exceeds 1 mm/year (Collier and Leeder, 1992; Armijo et al., 1996; Westaway, 2002; Leeder et al., 2003; Koukouvelas et al., 2005), suggesting that the faults studied have become progressively uplifted and exhumed.

The basement of the Corinth Rift consists of low grade metamorphic rocks, which are overlain by Pliocene to Quaternary clastic deposits (e.g. Ori, 1989; Xypolias and Koukouvelas, 2001). Basement lithologies appear in several nappes of the Miocene Hellenic fold and thrust belt, including Mesozoic limestone, shale, and greenschist and Tertiary flysch (Doutsos et al., 2000). Syn-rift cover deposits appear in several fault bound basins along the southern rift shoulder. They are mainly made up of continental facies rocks, such as colluvium, alluvium and fluvial deposits, grading into marine deposits towards the central rift (Ori, 1989; Doutsos and Piper, 1990; Dart et al., 1994; Malartre et al., 2004; Rohais et al., 2007).

3. Data acquisition

The fault core architecture of the two studied extensional faults was determined by detailed mapping of the fault surface

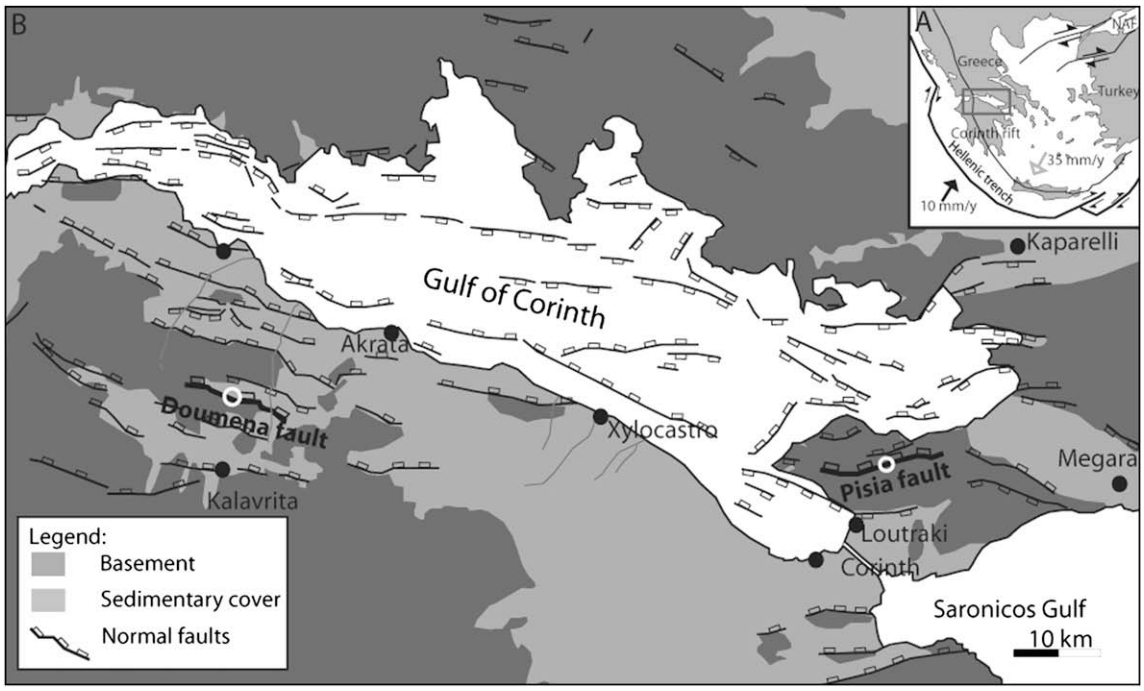

Fig. 1. A) Simplified tectonic map of the Aegean Sea, modified from Kokkalas and Doutsos (2001). B) Structural map of the Gulf of Corinth, modified from Moretti et al. (2003). The two studied faults are indicated by bold lines and circles.

morphology (principal slip surface) in parallel with describing and measuring the structural elements. The topology was established by use of topographical scan lines, oriented parallel and orthogonal to the strike of the fault, which were established by placing tightly stretched chords above the fault surface and reading the elevation from the surface to the chord (Fig. 2). The measurements were taken normal to the fault surface, with a regular interval of 0.1–0.5 m between each measurement. The scan lines were spaced 2–5 m, and in some cases, where the surface was particularly irregular, the profile distance was reduced accordingly and placed so the largest amplitudes were captured. The topological data were plotted on a map together with the position of surface intersecting structures such as fractures and fault lenses. Locally, small ravines that cut through the principal slip surface facilitate the study of the geometry and relations between the fractures and the distribution of fault rocks. In this contribution, fault rocks are classified according to the classification schemes proposed by Sibson (1977) and Braathen et al. (2004), with basis in outcrop observations, polished rock sections and thin section analysis.

The orientation and morphological characteristics of fractures of different types affiliated with the fault core (slip surfaces, smaller shear fractures, and joints) were classified according to Riedel's nomenclature (Riedel, 1929), namely as R-, R′-, Y- and P-shears and T-fractures by using the standard scheme for shear zones (Tchalenko, 1970; Petit, 1987). This analysis shows that the best developed fracture population is the fault-parallel Y-shears, R-shears and P-shears, of which the R-shears are steeper and the P-shears are more shallowly dipping than the Y-shears (Fig. 2). Fault lenses are elongate rock bodies that align with the master fault surface. They are bound on all sides by slip surfaces or fault rock layers and they consist either of protolith rock or of fault rock (Childs et al., 1996b; Gabrielsen and Clausen, 2001). Lenses can be classified according to size, orientation and relation to other lenses (Lindanger et al., 2007). Following Lindanger et al. (2007), the geometry of the fault lenses was quantified by measuring their principal axes (longest, intermediate and shortest) and comparing those to the strike of the master fault (b-axis) and the transport direction (c-axis). Further, lenses can be hierarchically arranged into orders, based on size and internal relationship.

3.1. The Doumena fault

The Doumena fault is one of a series of north-facing and basin bounding normal faults along the southern Corinth Rift shoulder. As for the other faults, the Doumena fault trends WNW-ESE and dips approximately 40–50° to the north. At the study site, the fault has a normal throw of c. 500 m, as documented by Poulimenos (1991) and Zygouri et al. (2008). Down-dip striations on the fault surface suggest an overall normal transport. The exposure at Doumena displays the principal slip surface and parts of the footwall (Figs. 3 and 4). The latter consists mainly of layered and folded low grade metamorphic carbonate of the pelagic Pindus Unit (Degnan and Robertson, 1998) that, in more detail, encompasses thick layers of grey, massive micritic limestone with some chert nodules, green marl, radiolarite, and some thin layers of siltstone. The hanging-wall displays poorly consolidate syn-rift conglomerate and sand layers of alluvial and fluvial origin, which can be ascribed to a Pliocene age (Malartre et al., 2004). Wedge-shaped units thinning away from the fault and possible unconformities illustrate their syn-rift status. The beds can also be seen to fold into a normal drag-fold close to the fault.

As seen in Fig. 4, the exposure reveals the principal slip surface, large parts of which is completely exposed. Dip angle and strike azimuths recorded along-strike- and dip-parallel scan lines reveal that the principal fault surface has a curved geometry and is characterized by ridges and troughs as seen both along-strike and down-dip (Fig. 5). The wavelengths of these features range from cm to hundreds of meters, whereas amplitudes range from a few cm to 2–3 m. The longest wavelength measured is dip-parallel and the shortest is strike-parallel (Figs. 4 and 5).

The geometry of the principal fault surface can be subdivided into three structural domains that form a gentle ramp-flat-ramp geometry in a down-dip (displacement parallel) section. The fault surface of the upper ramp and the middle flat are denoted domains

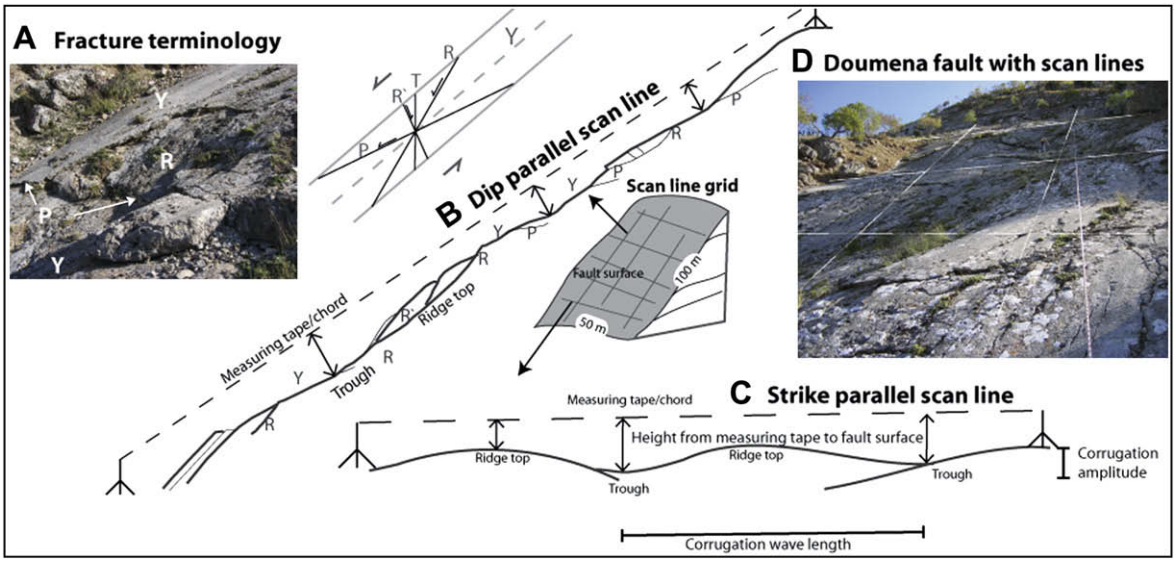

Fig. 2. Methods and terminology used in the mapping and descriptions of the two studied faults. A) Shear fractures, termed R, P, T and R′, with orientation and shear sense according to the principal slip surface (Y-shear). On the field photography, typical outcropping fracture surfaces are denoted. P-shears are seen as fracture traces truncating the Y- and R-shears and are therefore only seen as traces in the surface in this example. B) and C) illustratie construction of the scan lines. For descriptions of methods, see text. The scan lines are used to quantitatively describe the principal slip surface, and the distribution of lenses and secondary fractures. The constructed topographical grid is merged, to finally construct structural maps of the fault surface (see Figs. 4 and 9). D) illustrates the mapping grid lines of the surface of the Doumena fault. The picture is taken up slope toward south. Due to use of thin chords, they cannot be seen in this photograph, and dashed lines are instead drawn over to illustrate the position of the chords and the scan line grid.

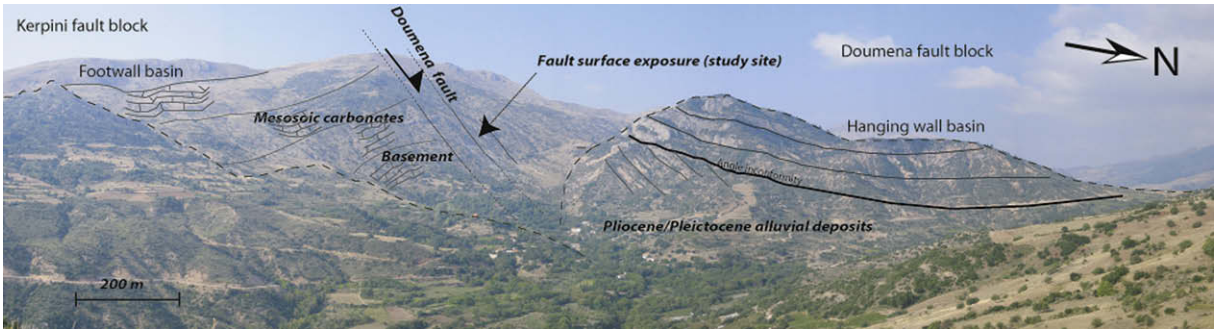

Fig. 3. The Doumena fault seen from the NE, contact between basement and basin fill is indicated. Note the inconformity and the normal drag in the half graben fill seen in the hanging wall of the Doumena fault.

DI and DII, respectively. They are dominated by an undulating, scoop-like geometry with an average dip (Y-shear orientation) of 50° for domain DI and 38° for domain DII. The dip-oriented scoops have wavelengths varying between 2 and 60 m and amplitudes of up to 2 m. In strike-parallel direction, curves have wavelengths from 1 m to 20 m, and amplitudes up to 2 m. Further analyses of these undulations reveal a systematic linear fit between amplitude and wavelength (Fig. 6B).

Domain DIII, which constitutes the lowermost ramp, has an upper boundary defined by a marked dip increase (from 38° to 60°) across a distinct, near-horizontal break line. This domain is characterized by several closely spaced parallel and planar slip surfaces distinctly different from the undulating geometry of the other two domains.

The undulating principal slip surface of domains DI and DII can be seen as one composite surface consisting of several separate slip surfaces, together defining the lower side of independent extensional lenses now removed by erosion (Fig. 7A,B,C). The upper and lower surfaces of these lenses are parallel to the Y-shears, whereas their up-dip and down-dip delineation surfaces best can be explained as R-shears and P-shears (Fig. 7A,B). These R- and P-shears occasionally cut and displace the principal slip surface (Fig. 7C). The largest lenses, which coincide with the larger wavelength and amplitude of the principal slip surface, are classified as 1st order lenses. The interior structuring of the lenses in many cases seems to be controlled by crosscutting R- and P-shears; consistent with duplexes with lenses of 2nd and 3rd order (see also Lindanger et al., 2007). The dimensions of the 1st order lenses range from 5 m to 48 m in the c-direction (parallel to transport), and 6–22 m in the b-direction (transverse to transport direction and parallel to fault strike) (Figs. 5 and 6). The 2nd and 3rd order lenses range from 1 m to 22 m in dip-parallel length, and from 2 to 12, 5 m in strike width. Generally, the majority of the 1st and 2nd order lenses have their longest axes oriented in the c-direction (parallel to dip and transport). When it comes to 3rd order lenses, some have equally sized b- and c-axes, perhaps indicating a different mechanism of generation compared to the larger lenses. Thickness (a-axis) of the 1st order lenses ranges from 0.6 to 1.2 m, whereas 2nd to 3rd order lenses generally have thicknesses of less than 0.5 m, although very few lenses where the a-axis could be measured with satisfactory certainty were available. Correlation of c- and b-axes data yield a very good linear fit (Fig. 6), no linear correlation was obtained when correlating b- and c-axes with a-axes (thickness).

Lithologically, three types of fault lenses are seen, namely those with protolith rock with preserved primary layering, those which consist entirely of fault rocks, and those that contain elements of both. It is of particular interest that lenses dominated by less deformed protolith rock are most common in the upper domain DII and are totally dominant in domain DI. Lenses dominated by fault rocks are common in domain DII. These lenses consist either of intensively fractured protolith rock or by smaller, better preserved protolith rock bodies surrounded by fault rocks (Fig. 7).

Lineation's defined by intersection between secondary shear fractures (R-, P, R′- and Y-shears) and the principal slip surface are frequent, and can be investigated in the third dimension in gullies. In such sections, one can distinguish between steeply dipping R-shears (50°–70° physical dip), shallowly dipping P-shears (20°–35° dip), Y-shears (35°–50° dip), and (antithetic) R′-shears (60°–80° dip) (Figs. 2, 3C, and 7A). Many R-shears have curved, cuspate shapes, and form the up-dip boundary of lenses. These R-shears typically displace the principal slip surface by 1 cm and 200 cm, with an average between 10 and 50 cm. Also P-shears commonly display curved fracture traces, shown by fracture intersection lines that curve up-slope. Locally, P- and R-shears are blind structures that die out in strike-direction. In some of these cases, they are associated with T-fractures that appear as en-echelon trails at the tip of the shears.

The rock volume of the fault lenses is crosscut by a dense network of smaller R-, P- and Y-shears. Also R′ fractures appear to be an important architectural element in many places (Fig. 7D). R′-shears are steep (70°–80°) and planar. Such fractures are observed on both the meter-scale (lenses) and the mm-scale (thin sections), and commonly occur in sets.

Two types of surface morphology of shear fracture can be identified, namely where striations affect the slip surface including slickenside lineation's, abrasion grooves, and abrasion tails, and smaller shear fractures displaying typically thin (sub-mm) fibrous growth of calcite. Abrasion tails are common and are found behind 1–2 cm chert clasts. The tails are made up of carbonate gouge and occur as 1–2 cm thick, 10–40 cm long and thinning tails on the down-dip side of particles. According to Means (1987), such abrasion tails are formed due to hard clasts acting as asperity ploughs in the slip surface, ploughing into the hanging-wall side during fault movement (see also Angelier, 1994).

Fault rocks most commonly appear in fault-parallel layers that are 0.5–3 m thick in lenses that are up to 2 m thick, or in thin membranes of 1–5 cm thickness (Fig. 7D,E). The fault rocks are subdivided into four types: (i) indurated clast-supported breccias, (ii) indurated matrix-supported breccias, (iii) non-cohesive clast-supported breccias, and (iv) gouge (nomenclature of Braathen et al., 2004). The indurated rocks dominate in domain DI and DII, while the non-cohesive rocks are more common in domain DIII. The fault rocks are strongly heterogeneous with up to 100 mm-sized clasts of fine-grained, gray, massive micrite, marly micrite and crystalline calcite embedded in a very fine-grained (<0.1 mm) matrix. Siltstone and chert act as accessory constituents. Both the clasts and the matrix consist of material that can be recognized to be derived from the protolith rock. One exception from this is the crystalline

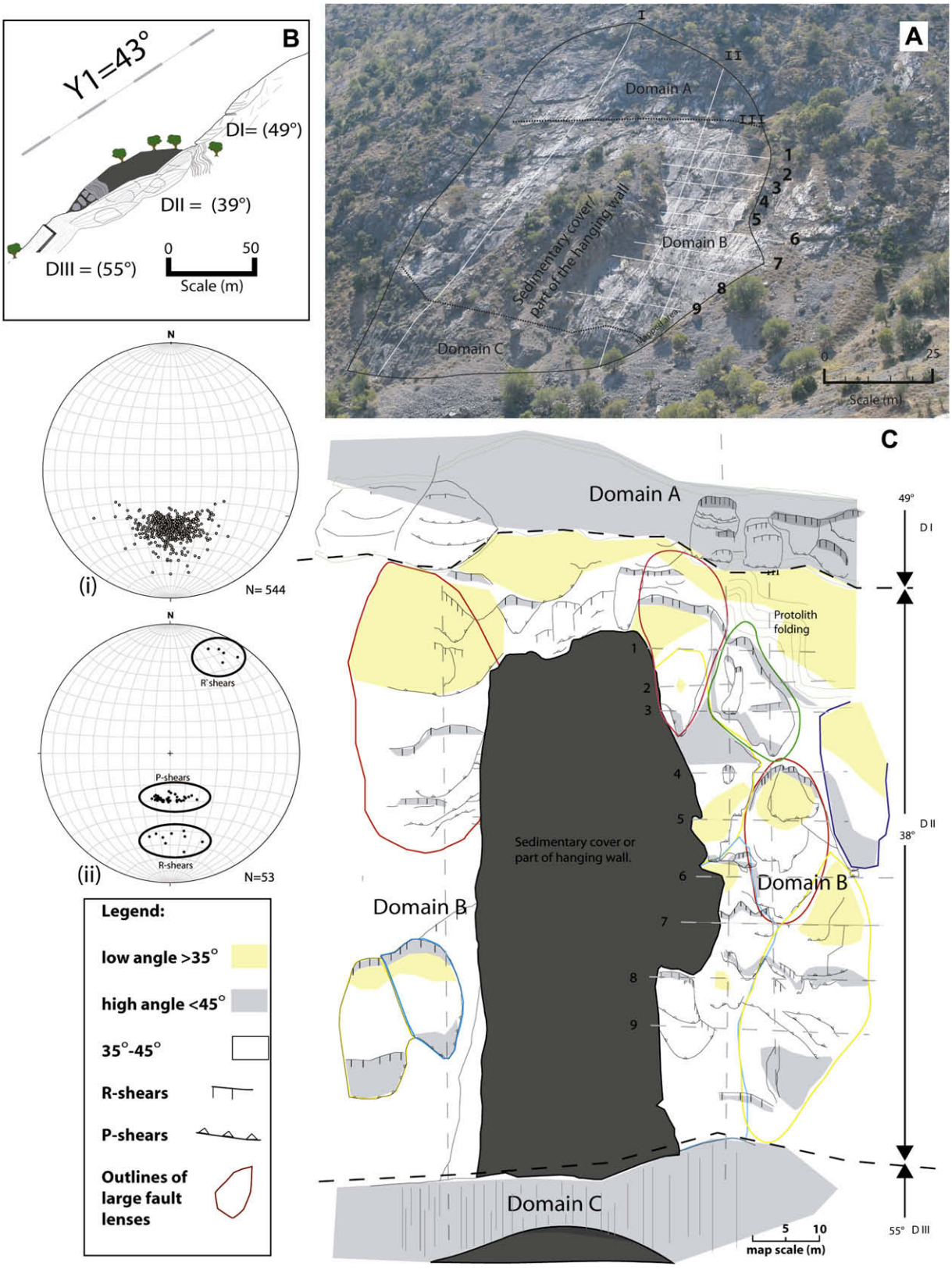

Fig. 4. A) View of the Doumena fault surface from the north. Scan line grid indicated by white lines. B) Schematic cross section of the Doumena fault surface, and its subdivision (domains DI–DIII). C) Structural map that shows structures on the fault surface, such as fractures and lenses from the fault surface. Position of pronounced fractures (R-, P- and Y-shears) are indicated. D) Stereo-plots of strike and dip measurements from the fault surface (pole to strike azimuth/dip in lower hemisphere, equal area stereo net). (i) Measurements from the undulating fault surface of all the three domains, revealing a mean orientation of 270/43 (pole to strike azimuth/dip in lower hemisphere, equal area stereo net). Orientation data were gathered in regular intervals along the scan lines. (ii) Measurements gathered of R, P and R′ fractures appearing at the fault surface.

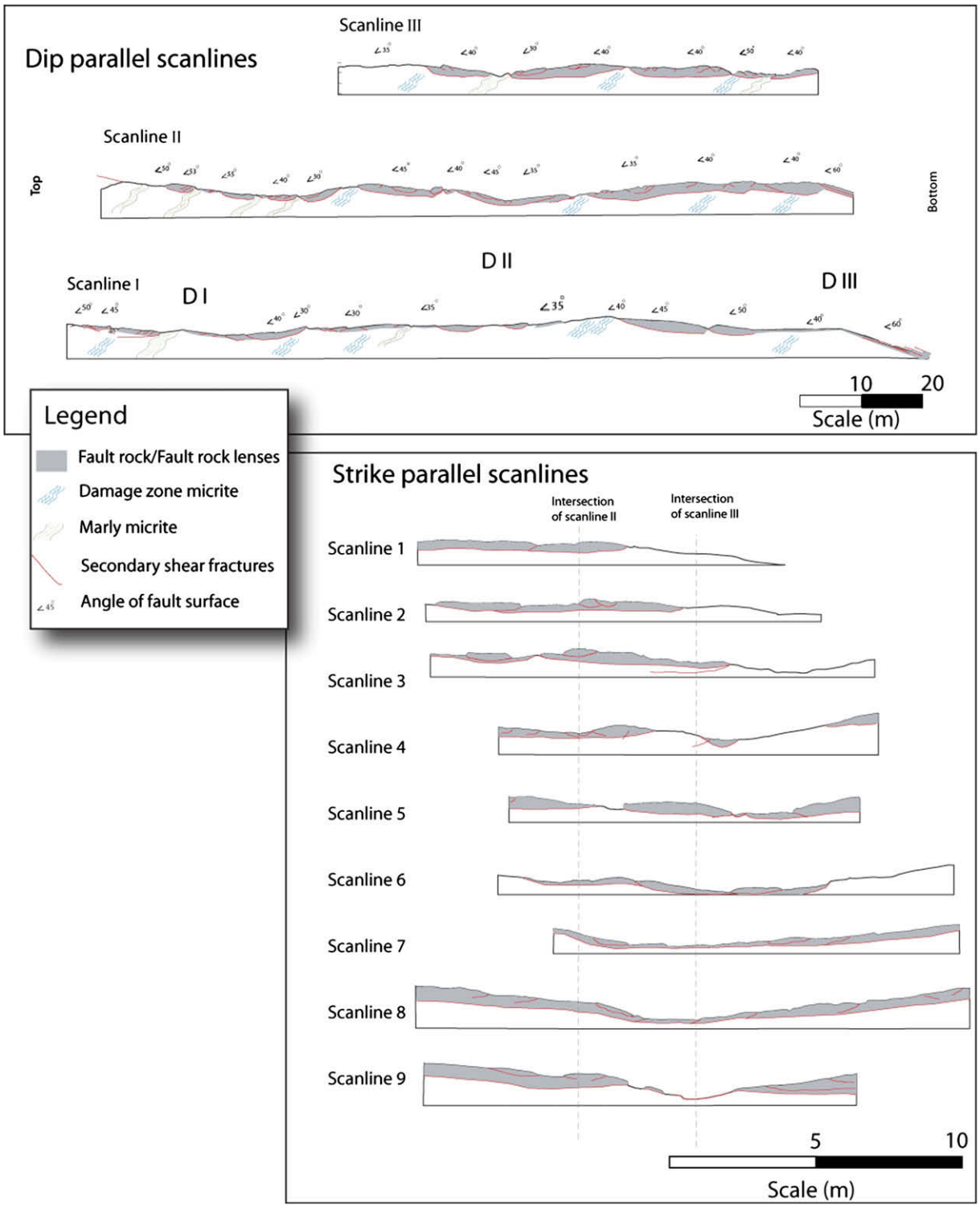

Fig. 5. Dip- and strike-parallel cross sections of the Doumena fault constructed along scan lines shown in Fig. 4A. Each scan line shows the topography of the fault surface and intersection of major fractures in the fault surface. Note that the vertical axes are exaggerated. The dip-parallel scan lines (I–III) show the overall geometry of the three domains (DI–DIII). The upper domain, DI, has an average inclination of 48°, and shows a wide scatter in orientation caused by curved slip surfaces. Furthermore, ridges and troughs oriented in the dip direction occur together with pronounced strike-parallel structures. The middle domain, DII (0–90 m), has an average dip angle of 38°. Here a curved slip surface (ridges and troughs) causes a wide scatter in orientation data. The lower domain, DIII (90–110 m in dip direction), has an average inclination of 55° and shows a planar geometry with parallel slip surfaces. Scan lines 1–9 show the strike-parallel fault surface morphology in domain DII.

calcite, which could be derived from cement precipitated in veins and voids in the fault rocks. The micritic host rock clasts are crosscut by stylolitic sutures, and calcite filled fractures. Stylolitic sutures in the protolith are formed due to Mesozoic compaction or as Labaume et al. (2004) suggest due to the Tertiary alpine folding. However, Labaume et al. (2004), also argues for pressure solution processes being active within the Quaternary faults of the Corinth rift, forming stylolitic structures at clast contacts between larger

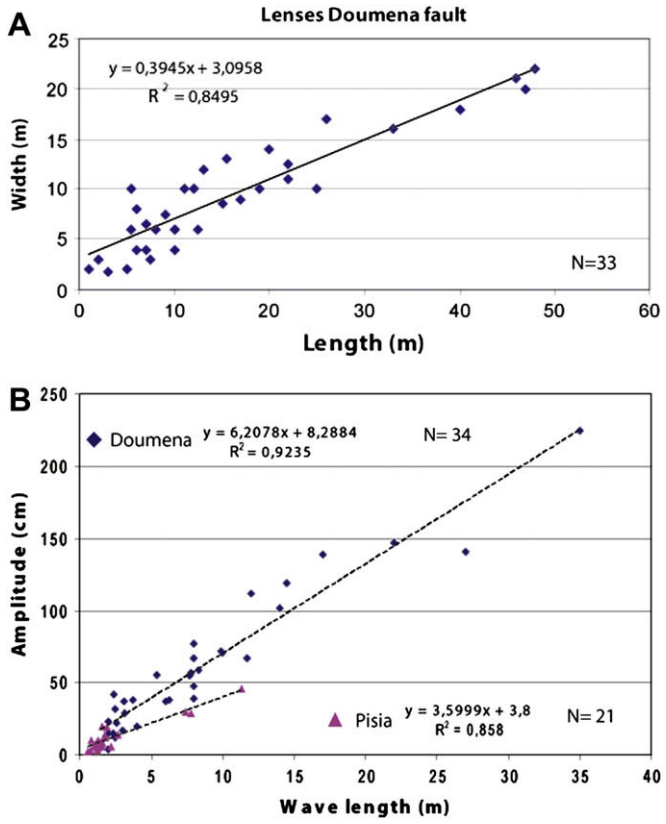

Fig. 6. X–Y plots of lens and corrugation dimensions, including a best-fit regression line for the datasets. A) Plot of the length (c-axis) and width (b-axis) relationship of all lenses from the Doumena fault. B) Plot that shows the width and thickness relationship of corrugation/undulations of the Doumena and Pisia faults in strike-direction. Note the difference in regression lines of the two datasets.

clasts. Such sutures are also observed in the fault rocks of Doumena fault.

Indurated clast-supported breccias (Fig. 8A,B) make up 1–20 cm thick layers surrounding lenses. In cases where lenses are associated with crosscutting thin slivers of matrix-supported breccia, fault rocks sometimes dominate the entire lens volume. In thin section the indurated clast-supported breccia appears as mostly massive, and consists of 1–10 mm elongate angular clasts of micrite (derived from the protolith rock) and twinned crystalline calcite. In many cases the larger clasts are cut by trans-granular microscopic R′ fractures that in places are filled with finer matrix grains. At the contact between the larger clasts, rust-coloured stylolitic sutures appear. Here, re-crystallized calcite cement is precipitated in the immediate vicinity of the stylolitic suture. Primary porosity of the breccias can reach 20–40%, especially where 0.5 mm size voids exists along the microscopic R′ fractures between angular clasts, but overall pore spaces are not found between clasts or in matrix.

Indurated matrix-supported breccias (Fig. 8C,D) appears in 1–10 cm thick layers most commonly associated with the major slip surfaces separating the fault lenses. This rock has sub-angular to rounded micrite and crystalline calcite clasts surrounded by a brown, fine-grained matrix. Larger clasts commonly have elliptical shapes with the long axis oriented parallel to the fault strike dimension, and the short axis parallel to the dip direction. In outcrops the rock has a massive appearance, but in thin sections from samples near the slip surface micro-layering can be seen as an anastomosing array of very fine-grained, gouge material, surrounding disc shaped clasts of micrite and crystalline calcite. This layering is subparallel to the slip surface indicating zones of higher degree of grain crushing.

Incohesive porous grain-supported breccias (Fig. 8E) appear together with bands of matrix-supported breccia and gouge, constituting meter-thick, dip-parallel fault rock beds. This unit is especially common in domain DIII. Grain-sizes vary from fine-grained in the matrix-supported breccia and gouge to course-grained in poorly sorted breccia, the latter hosting clast sizes of up to 30 cm. Such large clasts are found in the central part of the fault rock layer. The grain-supported breccias consist of sub-angular clasts of micrite and crystalline calcite surrounded by smaller grains. In this breccia pore spaces are abundant and can be up to 1–2 mm between larger clasts, supporting the incohesive state of this fault rock.

3.2. The Pisia fault

The Pisia fault is located to the eastern end of the Corinth Rift, and is hosted by a basement horst in the rift zone. At the study site, the Pisia fault trends E-W and dips 40° to the north with an estimated bulk normal throw of c. 400 m (Morewood and Roberts, 1999). The footwall is made up of Mesozoic marbles, Tertiary low grade flysch, and meta-volcanic and meta-sedimentary rocks associated with a dismembered ophiolite (Stewart and Hancock, 1991). At the studied locality the footwall consists of fine-grained, low-grade metamorphic micrite and the fault in places cuts cave precipitated calcite (flowstone). The hanging wall is covered by non-consolidated Quaternary colluvial and alluvial fan deposits (Leeder et al., 2002) (Fig. 9A).

The studied exposure of the Pisia fault is a 100 × 100-m principal slip surface of which an area of 50 × 50 m was mapped in detail using the scan line method as described above (Fig. 9B,C). Well-expressed striations and corrugation axes are consistent with an overall dip slip transport.

On the larger scale, the principal slip surface can be divided into two domains (PI and PII) based on lateral variations in dip angle and surface morphology, as shown in the strike- and dip-parallel scan lines (Figs. 9 and 10). Domain PI, which comprises most of the exposure, exhibits a composite slip surface that is characterized by a dense network of dip-parallel corrugations, causing undulation in strike-direction and planarity in dip direction. Domain PII is found near the western extent of the exposure and consists of a 4 m wide and 50 m long trough. The trough is filled by lenses, which are partly stacked on top of each other, producing a step-like geometry (Fig. 10, scan line II).

The surface morphology of domain PI is illustrated by five strike-parallel scan lines (Fig. 10), unravelling the geometry of corrugations. They are covered, bound, and crosscut by slip surfaces. Along strike, the corrugations have amplitudes ranging from 2 cm to 40 cm, and wavelengths ranging from 1 cm to 700 cm. Two size classes can be established, medium sized ridges (0.5–2 m wavelength) and large sized ridges (2–7 m wavelength). For both size domains, a plot of wavelength and amplitude (Fig. 6B) reveals a good linear relationship. On top of the corrugated surface there are slicken-lines, pit marks, and tool tracks (Sensu Hancock and Barka, 1987; Means, 1987).

Domain PII of the principal slip surface has a marked difference in surface geometry compared to domain PI. This is clearly displayed in scan line II, and in the right part of the horizontal scan lines (Fig. 10). The upper part of domain PII shows a trough with a planar base that gradually deepens down-dip. In the lower part of the trough there is a change into step-type geometry, characterized by steep curved fractures bounding fault lenses (Figs. 9 and 10, scan lines 1, 2 and II). In addition to Y-shears, the most common structures are R-shears and T-fractures; no P or R′-shears were observed.

The corrugated principal slip surface in domain PI is associated with an approximately 5–20 cm thick zone of intense strain,

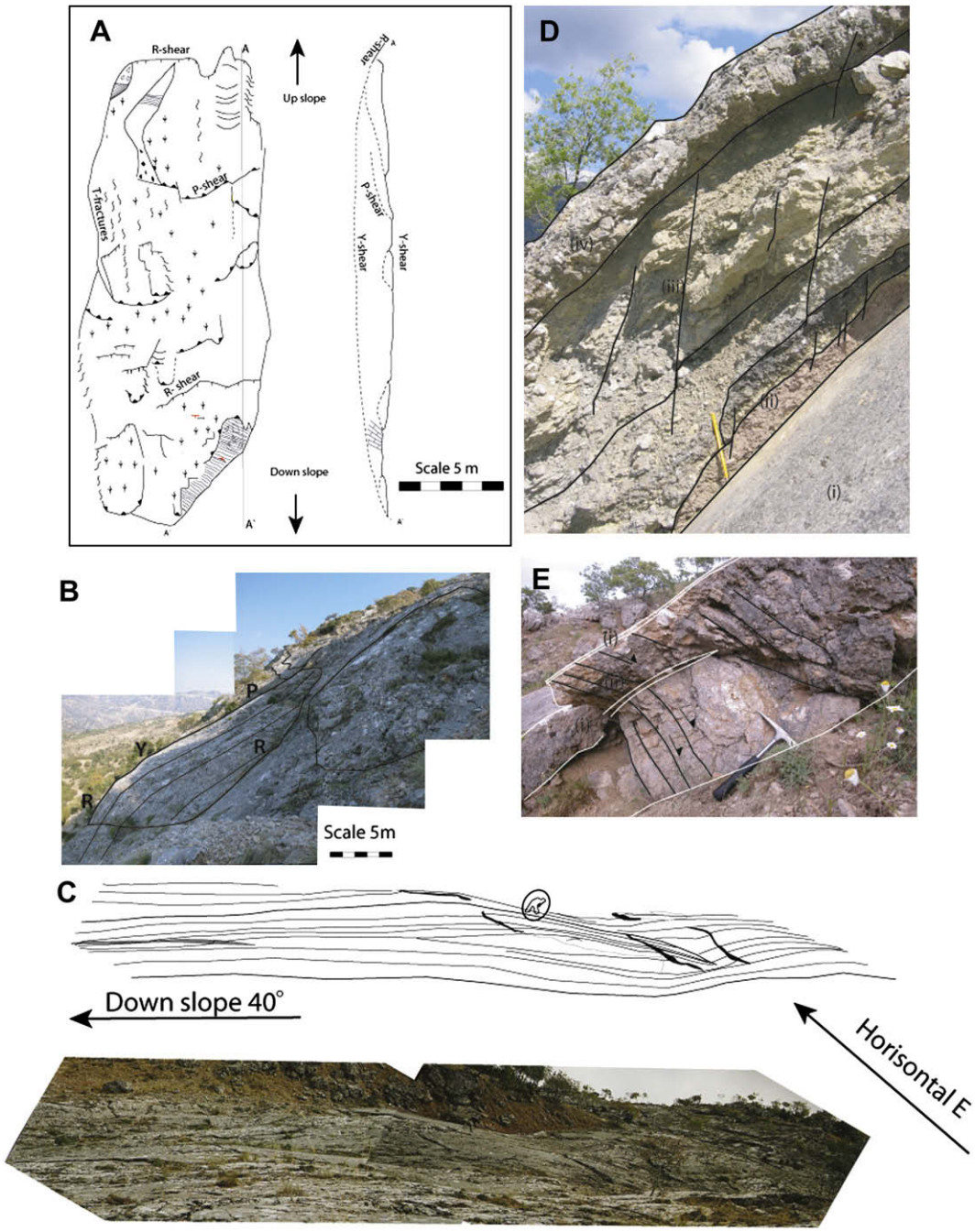

Fig. 7. Mesoscopic observations of the Doumena fault. A) Detailed map and dip section through a 2nd order lens. Note the steep R fractures and gently dipping P fractures that bound 3rd order lenses. B) and C) Outcropping lenses along fault surface of the Doumena Fault. C) highlights the topography the topography and lens stacking pattern. D) Internal architecture of a fault rock layer in domain DIII, showing (i) Planar fault surface, where the fault rock is a matrix-supported indurated breccia covered with abrasion tails (see text for description), (ii) layers of silt and graphite smeared along the fault surface, (iii) steep intragranular shear zones, cutting the fault rock layers, and (iv) layers of fault rocks in a composite membrane characterised by a grading of grain sizes, with the coarser rock in the middle. E) Vertical section in the fault core showing fault rocks and various shear structures occurring in fault core lens, including (i) membranes of indurated matrix-supported breccia, and (ii) lens that consists of indurated clast-supported breccia crosscut by R′ fractures. The lowermost part of the lenses consists of lightly deformed host rock.

consisting of a cluster of closely spaced slip surfaces (Fig. 10, scan line I). The frequency of these slip surfaces decreases to a total of 2–3 isolated Y-shears 3-m below the principal slip surface. The displacement measured across these features is minor (in the order of mm to cm) and no rotation of beds occurs. Neither are fault rocks associated with them. However, the rock volume between these fault branches is characterized by a network of steep (50°–70° absolute dip) R-shears with sigmoidal shapes. The R-shears either terminate as blind structures or they are interconnected to form continuous structures from one slip surface branch to another. Also, the Y-shears display minor displacement (mm to cm). T-fractures appear associated with the principal slip surface, and can constitute up to 15 m long continuous structures that are oriented obliquely (45°) to the fault surface dip line.

In domain PII, steeply dipping and curved R-shears dominate (Fig. 10, scan line II). In this domain they may be characterized by

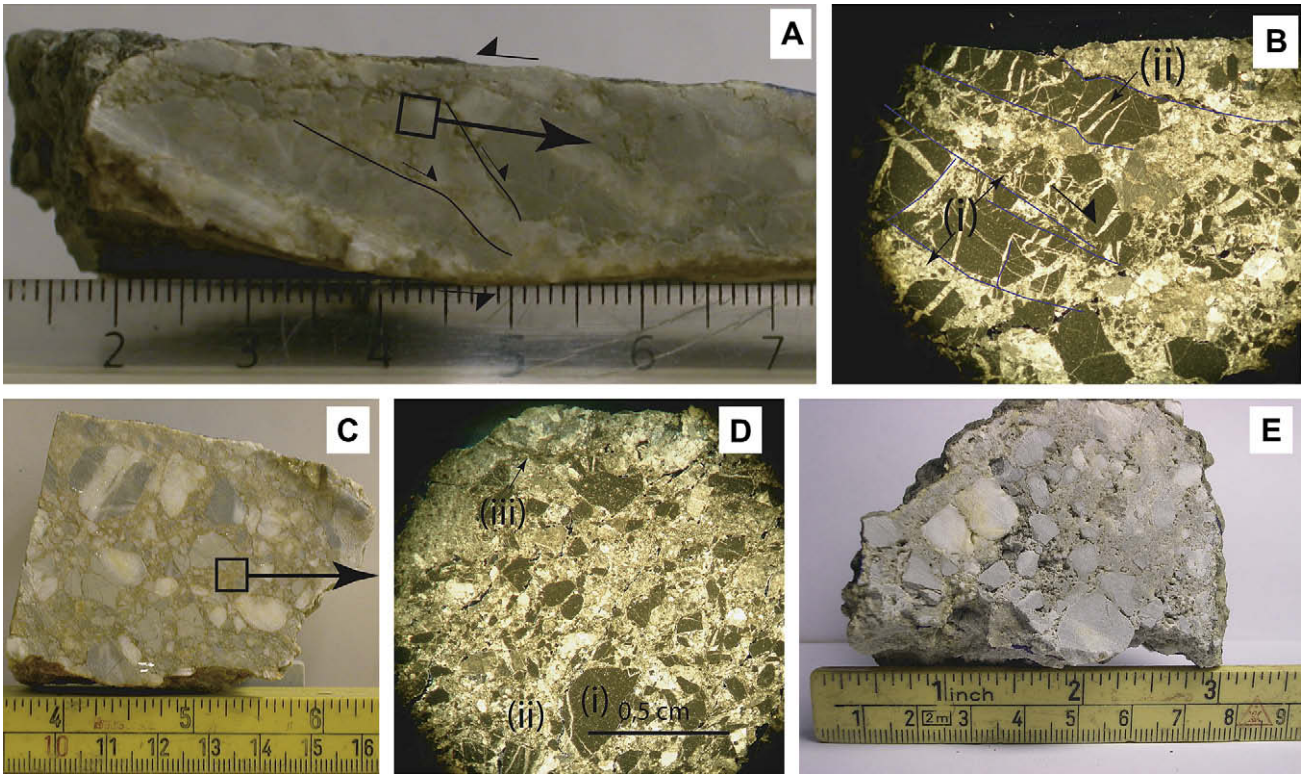

Fig. 8. Fault rocks of Doumena fault. A) vertical, polished section in clast-supported breccia. The rock is characterized by imbricate clasts separated by R-micro-shears. B) Photomicrograph of clasts-supported breccia. Clasts are angular and cut by trans-granular R′-shears: (i) trans-granular fractures are seen as zones of finely crushed micritic clast, and (ii) intra-granular tension fractures are filled with calcite cement oriented perpendicular to the trans-granular fractures. C) Photograph of a polished sample of an indurated matrix-supported breccia. Note the brown matrix surrounding the rounded to sub-rounded clasts. This rock appears mainly in 1–10 cm thick continuous to discontinuous layers surrounding the lenses. D) Photomicrograph of a matrix-supported breccia, showing (i) rounded micrite clast, (ii) fine-grained particles that make up the matrix, and (iii) thin planar clay laminae. E) Vertical polished section through a sample of a porous grain-supported breccia. This rock constitutes a thick membrane in domain DI. Note voids between the clasts and the low appearance of finer grained particles.

significant displacement, in one case an offset of more than 3 m of the principal slip surface is seen. They have a characteristic curved geometry in strike-direction, with a wavelength of up to 7 m and amplitude of 2 m, defining a curvature that has an opening angle of 70°. In dip direction the R-shears are planar.

Fault rocks in the Pisia fault differ from one structural domain to another. In domain PI tabular bodies of matrix-supported breccia and gouge occur, whereas wedge-shaped bodies and lenses are most common in domain PII (Fig. 10). The fault rocks differ from course-grained micrite dominated breccias to fine-grained crystalline calcite dominated breccias. The clast size differs from 10 to 100 mm in the course-grained micritic breccias to 1–2 mm in the fine-grained crystalline calcite breccias. As for the Doumena fault the micritic protolith rock is crosscut by stylolitic sutures, calcite filled veins, and fractures. However, the vein calcite seems to be derived from two different sources, namely the host rock itself and the speleothems. In thin section these are distinguished by that abundant crystal twinning is seen in the former, but rarely in the latter.

The domain PI fault encompasses three main rock units, of which the upper consists of ultra-breccia, the middle of nearly undeformed flowstone, and the lower unit of grey micritic breccia. The ultra-breccia is an *indurated matrix-supported breccia* (Fig. 11A,B). This rock makes up 5–20 cm thick layers covering the corrugated fault surface. The layers are separated by densely spaced and curved Y-shears creating lens-shaped bodies in the strike dimension and hence, defining the corrugations. Texturally, the rock contains grey, rounded and isometric 1–2 mm clasts of micrite, crystalline calcite and breccia totally surrounded by a fine-grained matrix appearing white in hand specimen and brown in thin sections. In thin sections the rock appears with thin zones of very fine-grained gouge cutting through areas of coarser breccias (Fig. 11C,D). These gouge zones correlate with the principal slip surfaces at the fault. Larger clasts of crystalline calcite show development of twinning, similar to type I and type II twins sensu Burkhard (1993), indicating low temperature during deformation.

The middle unit is a 1–3-m thick *flowstone* deposit (Fig. 11C,D). The flowstone consists of reddish white and grey crystalline calcite lamina that frequently envelope rock fragments of breccia and micrite. The orientation of the lamina is parallel to the principal slip surface (40° dip). In thin sections, the flowstone is seen to consist of thin crystals with growth direction perpendicular to the fault surface. Commonly, Y-shears cut the crystals, thereby forming 0.5 mm thick layers of brownish gouge. Twinning can sporadically be seen in fragmented calcite in the shear zones, but not within the undeformed elongated calcite crystals. This flowstone is described in detail by Roberts and Stewart (1994) who concluded that this rock was precipitated inside a cave during a karstic period. Thereafter the fault was reactivated along the cave, causing deformation in the flowstone.

The lowermost unit consists of a grey fault breccia, classified as a *matrix-supported micrite breccia* (Fig. 11D,E). This rock has a typical jigsaw texture of angular and partly re-crystallized micrite clasts, with the intra-crystalline space between the clasts filled with fine-grained micritic clasts. The matrix also fills trans-granular fractures in the larger clasts, suggesting that the fine-grained matrix was filtered out of the breccia and injected into fractures/

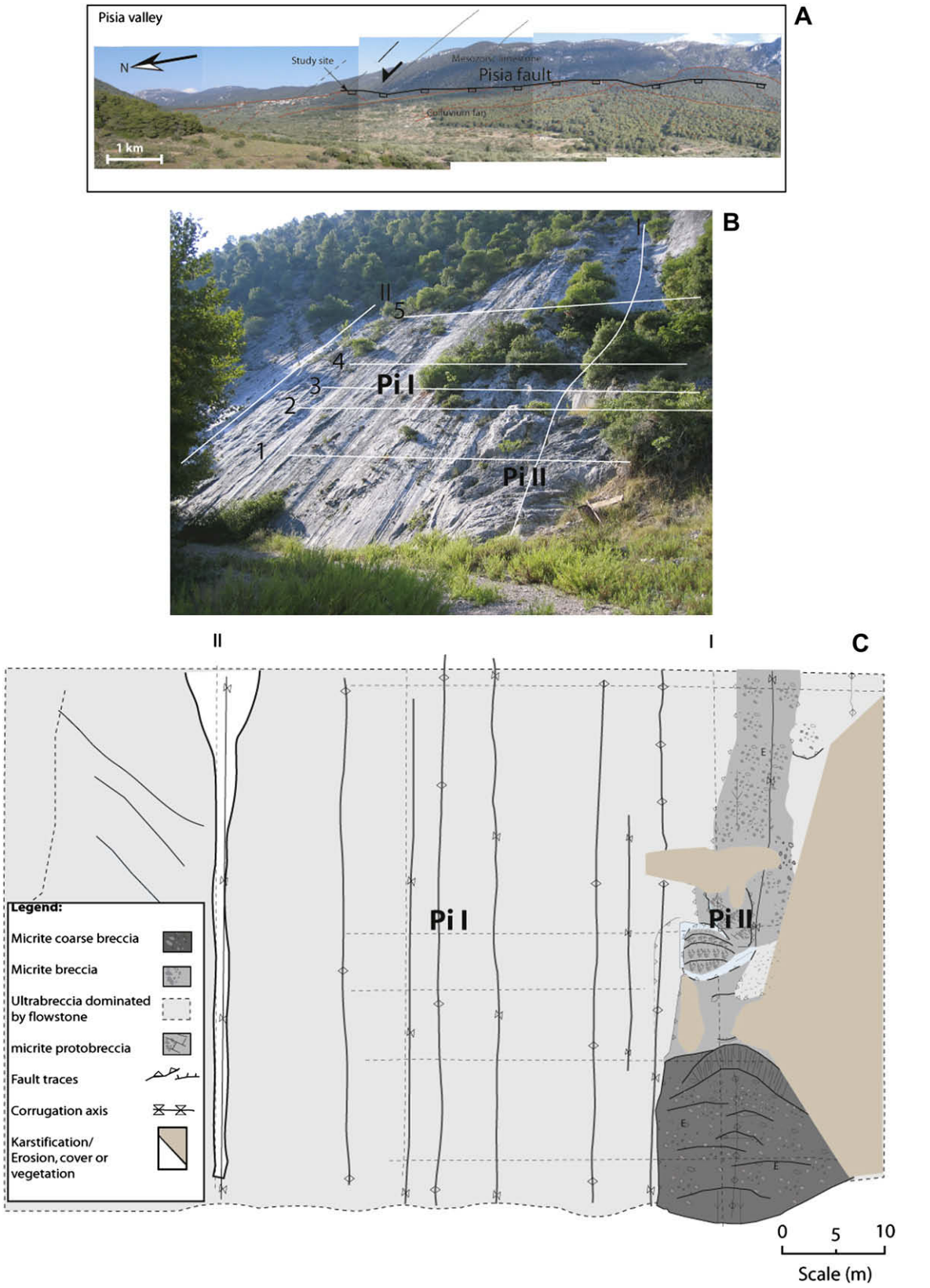

Fig. 9. A) Photo mosaic showing the Pisia fault scarp, with Mesozoic limestone in the ridge that make up the footwall, and colluvial and alluvial fans building into the hanging-wall basin. B) Photograph of the Pisia principal slip surface, showing the location of scan lines. C) Map of the principal slip surface, showing fault rock distribution and locating ridges and troughs of the corrugations.

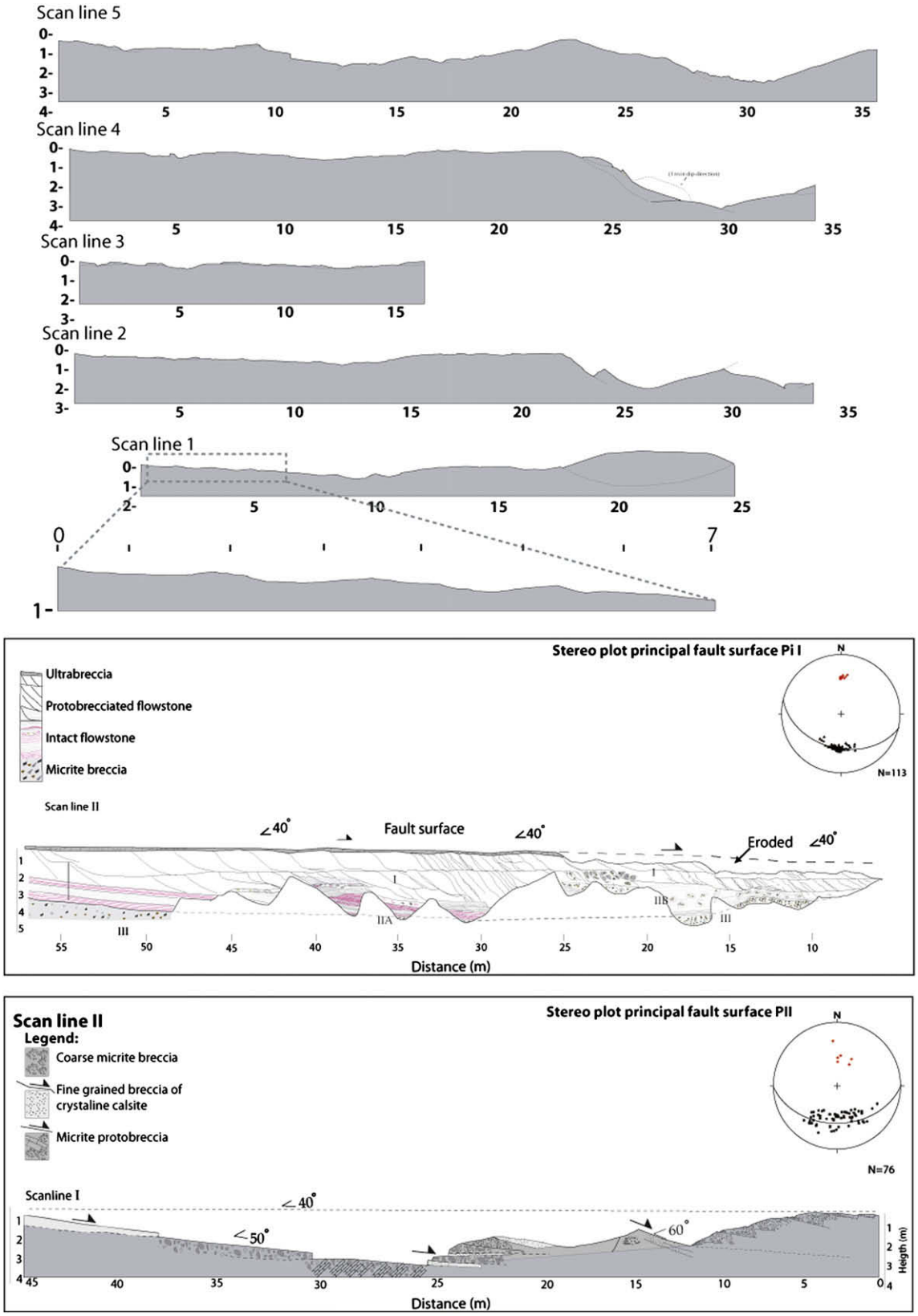

Fig. 10. Topographic cross sections of the Pisia principal slip surface. Scan lines 1–5 illustrate the strike-parallel topography of the fault surface. Scan lines I and II show both the fault topography and the distribution of fault rocks in domain PI and domain PII, respectively. Scan line I is constructed inside a gully in a 50-m long dip section, revealing the fault core. Rocks of the section can be divided into three parallel zones. Zone I is brecciated flowstone, zone II is intact flowstone, with subdivision A and B indicated by red and white flowstone, respectively. The lower zone III is dominated by micritic breccia. Orientation data are plotted as poles to planes. Note how surfaces of domain PII are less clustered than those of domain PI.

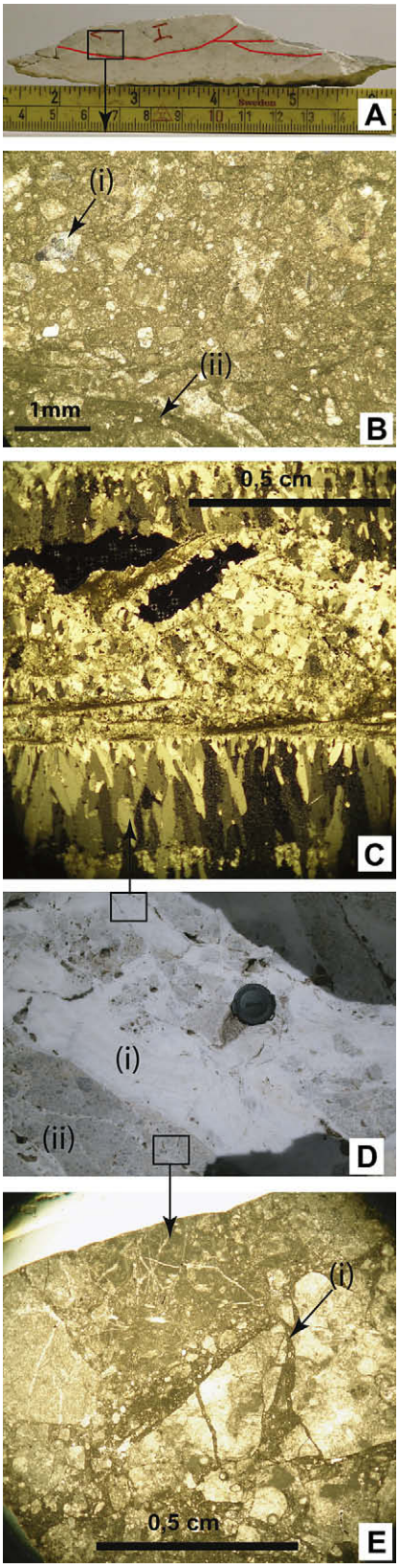

voids (Fig. 11B). According to Lin (1996), this is a process that is related to seismic events with brittle grain-size reduction and mobilization and injection of fine-grained gouge into areas of lower stress, like T-fractures.

In accordance with Roberts and Stewart (1994), we find that the upper ultra-breccia layer is younger and hosted in the flowstone. To the contrary, the breccia appearing underneath the flowstone is older and must have been formed before the cave was developed and the flowstone generated.

In domain PII, fault rocks are mostly composed of clast-supported breccia appearing as lenses or tabular bodies. The up-slope part of domain PII consists of several tabular bodies of fault rock, approximately 5–20 cm thick (Fig. 10, scan line II). Further down-slope in the part characterized by a step-like geometry, there are fault rock lenses and fault rock bodies with triangular shape. In contrast to domain PI, the rock type in the entire domain PII is dominated by micritic clast-supported breccias with no occurrence of flowstone. This rock is an *indurated clast-supported breccia* of micrite consisting of angular to sub-angular micrite grains in a brown fine-grained matrix. Clast size varies between 1 mm and 15 mm of the visible clasts, whereas grain sizes within the gouge is hard to distinguish based on thin section investigations. Voids in the breccia is partly filled by calcite characterized by low-grade type 1 twins (Burkhard, 1993). Compared to the other fault rocks of the Pisia fault, this breccia contains less cement. This may indicate that no flowstone was present in this area of the fault and that diagenesis has been moderate after the generation of the breccia.

4. Discussion

The presented dataset, which encompasses fault core geometry, general architecture of the fault zones and spatial distribution of fault rocks, can be used to unravel the development of the two faults and to shed light on the conditions that have contributed to the differences between them. The ultimate aim of the work is to produce a dataset that can be applied in geo-modelling and implicitly in the numerical investigation of fluid flow paths across and along carbonate-hosted fault cores (Tveranger et al., 2005; Fredman et al., 2007; Nøttveit et al., 2007).

4.1. Fault zone evolution

In order to investigate mechanisms behind observed structural elements of the Doumena and Pisia faults, the established overall architecture provides a good starting point. The Doumena fault is characterized by a gentle ramp-flat-ramp geometry, modified by segments of an undulating principal fault surface and the geometry of fault lenses in its upper part (domains DI and DII). In contrast, thick layers of fault rock cut by planar faults determine the geometry of its lower part (domain DIII) (Figs. 4 and 5). The development of a ramp-flat-ramp geometry can be explained by: (i) dip changes

Fig. 11. Fault rocks of the Pisia fault. A) Polished slab of a matrix-supported breccia of crystalline calcite. The red lines indicate shear fractures. The slab is cut parallel to strike and perpendicular to dip. B) Thin section of the matrix-supported crystalline breccia in Fig. 11A; showing (i) crystalline calcite clast with twinning, and (ii) shear zones within the breccia of very fine-grained particles in the matrix. These zones are parallel to the shear fractures indicated in Fig. 11A. C) Photomicrograph of a sheared flowstone. Shears are arranged in an en echelon pattern and consist of fine brown material. The shears cut the calcite crystals parallel to the growth cleavage. D) Photograph showing flowstone laminas enveloping clasts of micrite breccia in the upper part (i), and matrix-supported micrite breccia crosscut by cement-filled tension fractures (ii). E) Photomicrograph of the matrix-supported micrite breccia in Fig. 11D. Note how the finer matrix particles fill in trans-granular fractures in the larger micrite clast. This suggests that the matrix was injected into fractures.

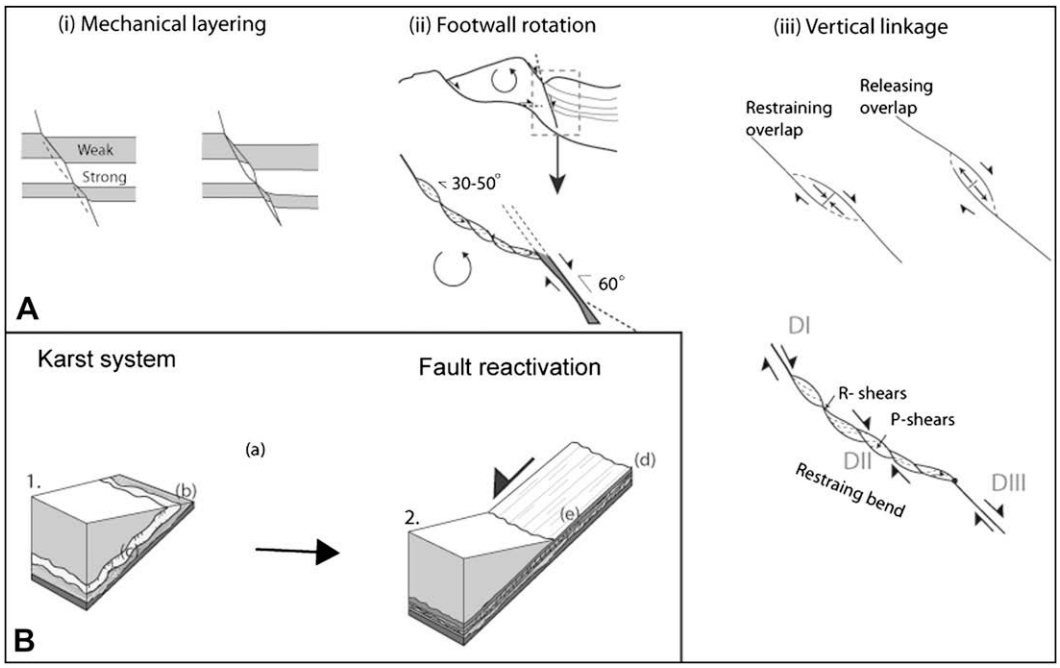

Fig. 12. A) The three stages in the development of the Doumena fault encompasses: (i) fracture propagation through a sequence with contrasting mechanical properties generates whiggly fault plane; (ii) rotation and reactivation of the master fault plane; and (iii) linkage of fault segments. B) Model for the development of domain PI of the Pisia Fault: a) old fault core, b) flowstone precipitated on top of older fault core, c) cave forming along the old fault core, d) new fault core formed after fault reactivation and collapse of the cave, and e) the development of a corrugated fault surface.

controlled by fault propagation through layers of contrasting mechanical strength, (ii) faulting during progressive rotation of the footwall block, or (iii) segment growth and linkage (Fig. 12A) (Childs et al., 1996a; Gabrielsen and Clausen, 2001).

The following observations are considered to be the most important in this respect: firstly, the carbonate host rock consists of layers with different mechanical strength (i.e. micrite, marl, and siltstone). Such variations often result in contrasting fracture orientation and, consequently, an irregular fault trace (Ferrill and Morris, 2003). Such irregularities may subsequently become sheared off by asperity bifurcation (Gabrielsen and Clausen, 2001) resulting in the generation of fault lenses. However, three aspects make the importance of this mechanism less likely: (i) the weaker layers such as marl and siltstone within the stronger micrite are fairly thin (up to 1 m) in accordance with the 500 m of displacement formed along the fault, and (ii) the protolith is also folded and deformed during Alpine deformation, and cannot as such explain the dip variations observed in the Doumena fault.

Secondly, the geometry of the Doumena fault could have been caused by a two-stage development, as proposed by Causse et al. (2004), a model, which is also supported by the existence of an angular inconformity in the hanging-wall syn-rift sediments (Fig. 3). Solheim (2002) demonstrated that the footwall block of the Doumena fault has undergone great rotation with bedding dipping more than 40° away from the Doumena fault. This would cause the Doumena fault progressively to rotate to a lower dip angle. In this model, domain DI and DII, which have lower dip angle than domain DIII, were developed first. After rotation of the footwall, renewed movement reactivated major parts of the fault zone, however, by the development of a more steeply dipping segment (domain III). At this stage, unroofing commence, bringing the fault to a shallower position. Hence, the contrasting characteristics of domains DI and DIII may be related to that they were developed at different levels of burial. Thus, the conditions for activity of domain III was characterized by higher confining pressure, resulting in the development of indurated fault rocks affected by pressure solution processes. In contrast, domain DIII was developed at shallower depth, with lower confining pressure, resulting in thick porous breccia layers associated with planar, parallel slip surfaces.

Thirdly, the ramp-flat-ramp geometry can be achieved through a vertical fault segment linkage process e.g. by growing fault segments forming restraining or releasing overlaps (Peacock, 2002; Rykkelid and Fossen, 2002). A restraining overlap zone would be associated with contraction that could cause the development of localized areas of a complex fracture networks. In such a case lenses may be generated by linkage of R- and P-shears, the latter of which would be required to link the two master fault segments. In domain DIII of the Doumena fault, lenses do not occur. Instead, parallel layers of porous breccia are found. In a ramp-flat-ramp model, this part represents the lower part of a releasing bend, focusing dilation (Tarasewicz et al., 2005). Since R- and P-shears are both truncating and displacing the principal slip surface, we consider the slip surface and the secondary shear fractures to be formed simultaneously during this linkage process.

The planar corrugated geometry of the Pisia fault is characteristic for several fault surfaces in the region (Hancock and Barka, 1987; Jackson and McKenzie, 1999). These authors argue that the planar geometry in the dip direction and the long extent of the corrugations are consistent with an incremental (stick-slip) mechanism. In such a model the initial undulating fault surface is formed by the propagation and linkage of curved fault segments (Ferrill et al., 1999). This implies that the early asperities became erased by the frictional, dip-parallel strain, whilst strike-parallel irregularities were preserved, since there are no movement in this direction. For the Pisia fault the appearance of flowstone in the footwall suggests that the fault core was rejuvenated in the presence of groundwater and that karstification took place (Roberts and Stewart, 1994). Since the flowstone laminae are oriented parallel to the fault (Fig. 10, scan line I), it is likely that the cave(s), where the

flowstone was precipitated, had a similar orientation. Based on dating of calcite cement, Roberts and Stewart (1994) suggest that the Pisia fault has been uplifted from sea level to today's level at 650 m in 2.2 My. During this period karstification due to meteoric water flow and subsequent flowstone precipitation took place.

4.2. Fault core elements

4.2.1. Principal slip surface geometry

Undulations of the principal slip surface are commonly ascribed to the mechanism of lateral propagation and linkage of segments (e.g. Ferrill et al., 1999). The Doumena fault displays undulations with wavelength up to 50 m in both dip- and strike-directions, whereas the Pisia fault has only strike directed undulations corrugations. Plots of wavelength against amplitude for the entire scale of lenses and corrugations show a good linear relationship (Fig. 6). This is consistent with previous work (Lee and Bruhn, 1996).

For the Doumena fault, the relationship between amplitude and wavelength has a much steeper gradient than for the same type of data from the corrugations in Pisia fault (Fig. 6B), perhaps reflecting that the fault surface undulations results from different mechanisms in the two cases. Accordingly, linkage of two separate segments possibly caused the large-scale undulations typical for the Doumena fault whereas fault propagation and segment linkage accompanied by collapse of a fault-hosted cavities may have been the driving mechanism for the development of the principal slip surface of the Pisia fault (see also Hancock and Barka, 1987). In the case of the Pisia fault, movement in the dip direction may have erased the dip-parallel asperities, while strike-oriented curvatures were preserved, since these structures did not act as obstacles to movement (e.g. McKenzie and Jackson, 1999). Furthermore, segmentation within the restricted karst-influenced area is likely to have controlled the amplitude of corrugations for the Pisia fault, since these are smaller than the similar structures of the Doumena fault. In limestone, the karst-weakening mechanism is most relevant and may be applicable for some restricted corrugated fault surfaces. However, the general picture is that the main displacement was accommodated as movement along a large, continuous slip surface, enhancing the development of dip-parallel corrugation structures.

4.2.2. Fault lenses

Lenses are developed by mechanism such as segment linkage, fault tip bifurcation or asperity bifurcation (Childs et al., 1996b; Gabrielsen and Clausen, 2001; Lindanger et al., 2007). The lens geometry found in the Doumena fault indicates that movement along crosscutting steeply dipping R-shears and low-angle P-shears are responsible for the lens development in the fault core, which is also suggested by Gèraud et al. (2006). The larger fault lenses are crosscut by R- and P-shears, bounding smaller lenses that are sometimes stacked to form duplexes (Fig. 7A). The length, width and thickness (c:b:a) relationship of the lenses gives an average of 32:19:1. Isolated length–width (c:b) relationships yield an average of 3:2, which is in good agreement with Bonson et al. (2007) who found values of 1.2:1–2.2:1 for the relation between c and b-axes axes in lenses of carbonate rocks. Lindanger et al. (2007) addressed the correlation on length vs. thickness of fault core lenses in different lithologies. They found an overall relationship of 12.5:1, between the slip-parallel (c) and shortest (thickness: a) axis. These values are significantly different for the data from this study, which gives a comparable 32:1 relationship. Since Lindanger et al. (2007) focused on faults with displacement of cm to c. 10 m, the discrepancy between datasets on lenses could relate to the extent of deformation; considering that the throws on the Doumena and Pisia faults are in the order of several hundred metres. For larger faults, lenses are likely to have undergone several episodes of collapse, will be more strongly abraded, and thereby are likely to become thinner (Lindanger et al., 2007). The difference in lens dimension is also likely to be strongly influenced by the variation in lithology and, hence, mechanical strength. Taken together, this suggests that lens dimensions may be self-similar within one fault or fault array, but are less likely to be so when faults with different cumulative displacement, strain rate and lithology are compared.

4.2.3. Fault rocks

Analysis of the fault rocks shows that the dominant mechanisms for generation of these rocks are brittle fragmentation and abrasion, resulting in clast-supported breccias and fine-grained matrix-supported breccias (Sammis et al., 1986; Handy, 1990; Braathen et al., 2004; Billi, 2005). Matrix-supported breccias dominate along the principal slip surface; while clast-supported breccias are more commonly related to secondary fracture systems like R-shears. The clast-supported breccias have the higher porosity of the two fault rock types, and particularly so in cases where fault rock layers are thick. Therefore, repeated faulting is likely to have controlled comminution, where the parts characterized by the most intense shear, generated a finer grain-size and lowered porosity.

4.3. Fault core model

A general model for the fault cores of the Doumena and Pisia faults is presented in Fig. 13. Three main components are included in the model: (i) fault lenses, (ii) tabular bodies of fault rock and cement, and (iii) slip surfaces. Fault lenses are characterized by an internal architecture of stacked, smaller, high-order lenses, formed by linkage of internal P- and R-shears. R′-shears frequently are seen to link synthetic fractures (P- and R-shears), which thus contribute to the development of fault lenses. Especially displacement along R′-shears seems to have been important for the rotation of fault lenses and for generating small pods of fault rocks. Internal shear and break-down of lenses are associated with generation of fault rocks, suggesting that lenses progressively deformed and broke down after their initial formation. Consequently, the lithology and internal structure of the fault lenses vary from those that are less deformed to those more strongly deformed. The lithology is ranging from almost undeformed protolith rock to completely dominated by fault rocks. Furthermore, fault rocks reveal higher porosity in central parts of the fault lenses as compared to the sheared lens-margins. Fault rock layers and pods also are found to be distributed along the principal slip surface, probably due to distributed wall rock abrasion, and in releasing bends of the fault core. In the latter case stress gradients may have caused flow of fault rocks into preferred positions.

4.4. Implications of fault architecture for fluid flow

In carbonates, fault cores are considered as an obstacle to fluid flow, while the damage zone is regarded as a conduit for flow (Cello et al., 2001; Cello et al., 2003; Micarelli et al., 2003; Micarelli et al., 2006b). Fractures are therefore generally considered to be the most important fluid conductor in these rocks. However, in carbonate rocks cementation by secondary precipitation of calcite in fractures is common, especially along and close to the fault core, contributing to reduced fluid conductivity (Micarelli et al., 2006a; De Paola et al., 2007). Also cementation is enhanced in areas of high pressure solution (Carrio-Schaffhauser and Gaviglio, 1990; Labaume et al., 2004) and in areas of high fluid percolation (Cello et al., 2001), whereas fine-grained fault rocks and smearing of fine-grained fault rocks or shale protoliths along the fault cores also contribute to sealing (Yielding

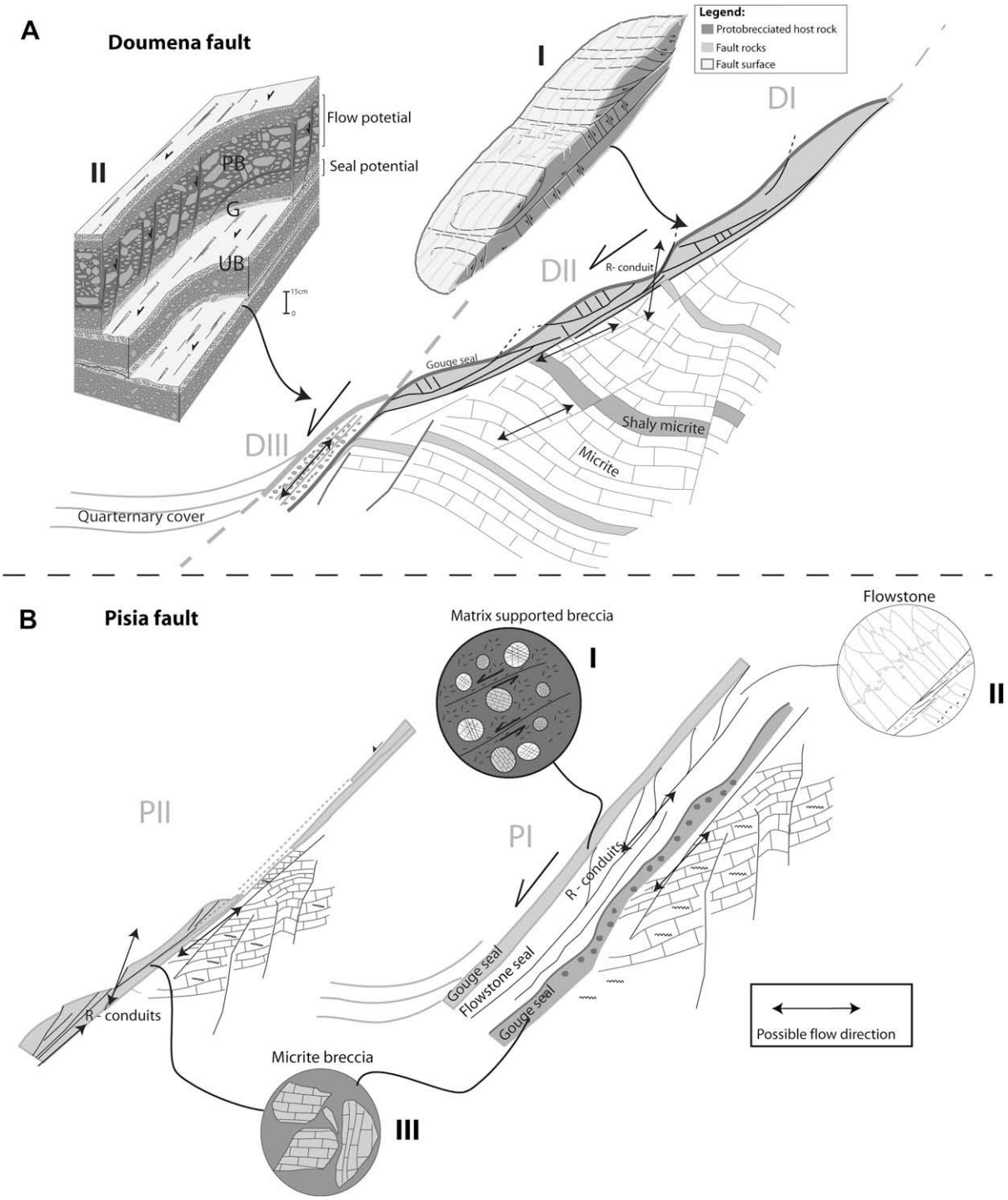

Fig. 13. Generalized models illustrating the architecture and the possible permeability as related to structural features of the cores of Doumena and Pisia faults. A) The Doumena fault core consists of mainly two elements, fault lenses and a fault rocks layers. Obstacles to fluid flow are matrix-supported fault rocks, while fractures, principal slip surfaces and porous fault rocks are considered pathways for fluids. I: Generalized geometry of fault core lens and the geometrical relationship between main fracture types. The lenses are surrounded by discontinuous fault rock membranes. R shears and P shears are truncating the principal slip surface forming lenses, and may therefore be pathways for fluids across or at least increasing the internal permeability of the fault core. II: Internal structure of a fault rock layer where several layers are separated by slip surfaces. Ultra-breccia (UB) and gouge (G) dominate along the slip surfaces while porous breccias (PB) constitute the central part of the layers. B) The Pisia fault consists of fault-parallel layers of flowstone and fault rock layers of mostly matrix-supported breccias. The fault core architecture favours fluid flow to occur along the principal slip surfaces and along damage zone fractures. Across the fault both fault rocks and cementation will act as seal.

et al., 1997). On the other side, Gèraud et al. (2006) suggested that networks of R- and P-shears could enhance flow in the fault core. This is observed in the Pirgaki fault, a fault situated north of the Doumena fault at the southern shore of the Gulf of Corinth. It is here argued that the morphology of the fracture surface controls the flow. Especially R-shears, which have smooth surfaces are favourable to promote fluid flow, in contrast to the P-shears that have a more serrated morphology. This is especially relevant for intrinsic communication in

and across fault zone lenses and duplexes. Also, lenses in direct contact can juxtapose areas of potentially high conductivity. Another important aspect is the development of karst structures along fault cores. During karstification and subsequent flowstone precipitation, fluids may have circulated over long distances along the fault core, forming channels of ultra-high permeability.

As discussed above, the Doumena and Pisia faults comprise two opposite geometries, one with dominantly undulating and segmented geometry (Doumena fault) and one with a planar geometry for the (Pisia fault). Fig. 13 illustrates possible fluid flow patterns considered here for the studied faults.

The flow potential inside the fault core of the planar Pisia fault is controlled by the thick cement and fault rock seals formed within the fault core, which restricts the transversal fluid flow. Apart from some R-shears, the major fluid flow patterns are likely to be concentrated parallel to the fault, along the Y-shears (parallel to dip). The R-shears may, however, increase the interconnectivity of the principal slip surfaces. The development of karst supports the interpretation that the principal slip surfaces may have had a large impact on fluid flow direction at an early stage of fault development. For the Doumena fault a well-developed R, R′, P and T fracture framework formed in the core, together with parts of porous breccias may give higher permeability across fault. Therefore, the permeability may be even more enhanced in the fault core, however depending on the footwall protolith from where the fault core material was derived. The DIII domain is characterized by parallel shear fractures similar to that of the Pisia fault, but has also a thicker volume of porous breccia. The shear zones consist of finer breccias and gouge and will provide seals with a potential to focus the fluid flow parallel to the fault core. In contrast, the DI and DII domains consist of more indurated fault rocks, with a possible fracture-controlled permeability. The connectivity is high, cause of lens formation by the inter-linkage of R and P-shears, and further fracturing by R′-shears within the lenses. Both R and P-shears are in many cases truncated by the Y-shears interrupting the seals associated with the principal slip surface and potentially juxtaposing units of more porous fault rocks.

As suggested by several authors working in "the Corinth rift laboratory" (e.g. Micarelli et al., 2003; Cornet et al., 2004; Labaume et al., 2004; Micarelli et al., 2006b) the fault fluid flow patterns are governed by the inner damage zone in that the fault core provides an obstacle to fluid flow. In our study of the morphology of the principal slip surfaces and internal structure of the fault core, we observe that there are at least two different core types, one of which is associated with planar segments. These are characterized by wide transversal barriers and an excellent permeability parallel to the fault, as also indicated by a well-developed karst systems. The second type is affiliated with faults with undulating slip surfaces, which are characterized by complex interior fault core architecture, and dominated by fault lenses and shear fracture networks. The latter type of fault core architecture may enhance the across fault and interior fault core fluid flow. Therefore, faults with this geometry might represent possible leakage points in reservoirs.

5. Conclusions

From the study of the architecture of two extensional faults in micritic carbonate, the Doumena and Pisia faults (Corinth, Greece), it can be concluded that

1) Main elements in carbonate fault cores are principal slip surfaces, layers and lenses of fault rock and protolith, corrugations, minor shear fractures, and tension fractures.
2) Fault segments with irregular geometries, including bends and jogs develop more complex fault core architecture than planar segments and frequently host lenses, some of which have enhanced porosity, and complex networks of interconnected fractures.
3) Lenses in fault bends can be ascribed to formation of R-shears and P-shears.
4) In planar fault segments, a corrugated fault surface with an associated thin high-strain zone is formed. Corrugation is a clear indication of movement along the same surface over many fault increments.
5) Lenses in the Doumena fault have an average length–width relationship of 3/2.
6) Principal slip surfaces of the two faults studied have strike-parallel undulations with a fairly similar aspect ratio of amplitude vs. wavelength (1:19 and 1:14), even though there is a striking difference in down-dip geometry.
7) The style of deformation in fault bends or breached relays of micritic carbonate rocks suggests that this part of the fault core is an important pathway for fluid flow.
8) A tentative model for fluid flow in micritic fault cores suggests that fluid pathways is parallel to fault core in planar fault, while in fault bends, fractures and lenses increase the possible across fault flow.

Acknowledgements

The authors thank Einar Sverdrup for introducing the field area and Morten Solheim and Jan Tveranger for guidance and fruitful discussion during field work. Atle Rotevatn and Nestor Cardozo are thanked for critical reviews and discussion during early stages of the writing of this paper. The contents of this paper benefited significantly through careful reviews by Ioannis K. Koukouvelas and an anonymous reviewer. The study was financed by the Fault Facies project at the Centre for Integrated Petroleum Research, University of Bergen by support from ConocoPhillips, StatoilHydro, and the Norwegian Research Council.

References

Angelier, J., 1994. Fault slip analysis and palaeostress reconstruction. In: Hancock, P.L. (Ed.), Continental Deformation. Pergamon Press, pp. 55–100.
Armijo, R., Meyer, B., King, G.C.P., Rigo, A., Papanestassiou, D., 1996. Quaternary evolution of the Corinth rift and its implications for the late Cenozoic evolution of the Aegean. Geophysical Journal International 126, 11–53.
Billi, A., 2005. Grain size distribution and thickness of breccia and gouge zones from thin (<1 m) strike-slip fault cores in limestone. Journal of Structural Geology 27, 1823–1837.
Bonson, C.G., Childs, C., Walsh, J.J., Schopfer, M.P.J., Carboni, V., 2007. Geometric and kinematic controls on the internal structure of a large normal fault in massive limestones: the Maghlaq Fault, Malta. Journal of Structural Geology 29 (2), 336–354.
Briole, P., Rigo, A., Lyon Caen, H., Ruegg, J., Papazissi, K., Mistakaki, C., Balodiumou, A., Veis, G., Hatzfeld, D., Deschamps, A., 2000. Active deformation, of the gulf of Korinthos, Greece: results from repeated GPS surveys between 1990 and 1995. Journal of Geophysical Research 105 (No. B11), 25605–25625.
Braathen, A., Osmundsen, P.T., Gabrielsen, R.H., 2004. Dynamic development of fault rocks in a crustal-scale detachment: an example from western Norway. Tectonics 23 (No. 4 TC4010), 1–21.
Burkhard, M., 1993. Calcite twins, their geometry, appearance and significance as stress–strain markers and indicators of tectonic regime: a review. Journal of Structural Geology 15 (3–5), 351–368.
Caine, J.S., Evans, J.P., Forster, C.B., 1996. Fault zone architecture and permeability structure. Geology 24, 1025–1028.
Carrio-Schaffhauser, E., Gaviglio, P., 1990. Pressure solution and cementation stimulated by faulting in limestones. Journal of Structural Geology 12 (8), 987–994.
Causse, C., Moretti, I., Eschard, R., Micarelli, L., Ghaleb, B., Frank, N., 2004. Kinematics of the Corinth Gulf inferred from calcite dating and syntectonic sedimentary characteristics. Comptes Rendus Geosciences 336 (4–5), 281–290.
Cello, G., Tondi, E., Micarelli, L., Invernizzi, C., 2001. Fault zone fabrics and geofluid properties as indicators of rock deformation modes. Journal of Geodynamics 32 (4–5), 543–565.
Cello, G., Tondi, E., van Dijk, J.P., Mattioni, L., Micarelli, L., Pinti, S., Niewland, D.A., 2003. Geometry, kinematics and scaling properties of faults and fractures as tools for modelling geofluid reservoirs: examples from the Appennines, Italy.

In: New Insights into Structural Interpretation and Modelling. Geological Society, London, Special Publications, vol. 212 7–22.
Chambon, G., Schmittbuhl, J., Corfdir, A., Orellana, N., Diraison, M., Geraud, Y., 2006. The thickness of faults: from laboratory experiments to field scale observations. Tectonophysics 426 (1–2), 77–94.
Chester, F.M., Evans, J.P., Biegel, R.L., 1993. Internal structure and weakening mechanisms of the San Andreas Fault. Journal of Geophysical Research 98 (B1), 771–786.
Chester, F.M., Logan, J.M., 1986. Composite planar fabric of gouge from the Punchbowl fault zone, California. Journal of Structural Geology 9, 621–634.
Childs, C., Nicol, A., Walsh, J.J., Watterson, J., 1996a. Growth of vertically segmented normal faults. Journal of Structural Geology 18, 1389–1397.
Childs, C., Walsh, J.J., Watterson, J., 1997. Complexity in fault zone structure and implications for fault seal prediction. In: Møller-Pedersen, P., Koestler, A.G. (Eds.), Hydrocarbon Seals: Importance for Exploration and Production. (Elsevier) Norwegian Petroleum Society Special Publication, vol. 7, pp. 61–72.
Childs, C., Watterson, J., Walsh, J.J., 1996b. A model for the structure and development of fault zones. Journal of the Geological Society of London 153, 337–340.
Clausen, J.A., Gabrielsen, R.H., Johnsen, E., Korstgård, J.A., 2003. Fault architecture and clay smear distribution. Examples from field studies and drained ring-shear experiments. Norwegian Journal of Geology 83 (2).
Collier, R.E.L., Leeder, M.R., 1992. Rates of tectonic uplift in the Corinth and Megara Basins, Central Greece. Tectonics 11 (6), 1159–1167.
Cornet, F.H., Bernard, P., Moretti, I., 2004. The Corinth Rift Laboratory. Comptes Rendus Geosciences 336 (4–5), 235–241.
Dart, C.J., Collier, R.E.L., Gawthorpe, R.L., Keller, J.V.A., Nichols, G., 1994. Sequence stratigraphy of (?) Pliocene-Quaternary synrift, Gilbert-type fan deltas, northern Peloponnesos, Greece. Marine & Petroleum Geology 11 (5), 545–560.
De Paola, N., Collettini, C., Faulkner, D.R., Trippetta, F., 2008. Fault zone architecture and deformation processes within evaporitic rocks in the upper crust. Tectonics 27 (TC4017).
De Paola, N., Collettini, C., Trippetta, F., Barchi, M.R., Minelli, G., 2007. A mechanical model for complex fault patterns induced by evaporite dehydration and cyclic changes in fluid pressure. Journal of Structural Geology 29 (10), 1573–1584.
Doutsos, T., Kokkalas, S., 2001. Stress and deformation patterns in the Aegean region. Journal of Structural Geology 23 (2–3), 455–472.
Doutsos, T., Koukouvelas, I., Poulimenos, G., Kokkalas, S., Xypolias, P., Skourlis, K., 2000. An exhumation model of the south Peloponnesus, Greece. International Journal of Earth Sciences 89 (2), 350–365.
Doutsos, T., Piper, D.W., 1990. Listric faulting, sedimentation and morphological evolution of the Quaternary eastern Corinth rift, Greece: first stages of continental rifting. Geological Society of America 102, 812–829.
Doutsos, T., Poulimenos, G., 1992. Geometry and kinematics of active faults and their seismotectonic significance in the western Corinth-Patras rift (Greece). Journal of Structural Geology 14, 689–699.
Evans, J.P., Forster, C.B., Goddard, J.V., 1997. Permeability of fault-related rocks, and implications for hydraulic structure of fault zones. Journal of Structural Geology 19 (11), 1393–1404.
Ferrill, D.A., Morris, A.P., 2003. Dilational normal faults. Journal of Structural Geology 25 (2), 183–196.
Ferrill, D.A., Stramatakos, J.A., Sims, D., 1999. Normal fault corrugation: implications for growth and seismicity of active normal faults. Journal of Structural Geology 21 (8/9), 1027–1038.
Flotté, N., Sorel, D., 2001. Structural cross sections through the Corinth-Patras detachment fault-system in Northern Peloponnesus (Aegean Arc, Greece). Bulletin of the Geological Society of Greece XXXIV/1, 235–241.
Fredman, N., Tveranger, J., Semshaug, S.L., Braathen, A., Sverdrup, E., 2007. Sensitivity of fluid flow to fault core architecture and petrophysical properties of fault rocks in siliciclastic reservoirs: a synthetic fault model study. Petroleum Geoscience 13, 305–320.
Gabrielsen, R.H., Clausen, J.A., 2001. Horses and duplexes in extensional regimes: a scale-modelling contribution. In: Koyi, H.A., Mancktelow, N.S. (Eds.), Tectonic Modelling: A Volume in Honor of Hans Ramberg. Geological Society of America Memoir 193. Geological Society of America, Boulder, pp. 207–220.
Geraud, Y., Diraison, M., Orellana, N., 2006. Fault zone geometry of a mature active normal fault: a potential high permeability channel (Pirgaki fault, Corinth rift, Greece). Tectonophysics 426 (1–2), 61–76.
Gibbs, A.D., 1983. Balanced cross-section construction from seismic sections in areas of extensional tectonics. Journal of Structural Geology 5, 153–160.
Goldsworthy, M., Jackson, J., Haines, J., 2002. The continuity of active fault systems in Greece. Geophysical Journal International 148, 596–618.
Hancock, P.L., Barka, A.A., 1987. Kinematic indicators on active normal faults in Western Turkey. Journal of Structural Geology 9 (5–6), 573–584.
Handy, M.R., 1990. The solid-state flow of polymineralic rocks. Journal of Geophysical Research 95 (B6), 8647–8661.
Hubert, A., King, G., Armijo, R., Meyer, B., Papanastasiou, D., 1996. Fault re-activation, stress interaction and rupture propagation of the 1981 Corinth earthquake sequence. Earth and Planetary Science Letters 142 (3–4), 573–585.
Jackson, J., McKenzie, D., 1999. A hectare of fresh striations on the Arkitsa Fault, central Greece. Journal of Structural Geology 21 (1), 1–6.
Jackson, J.A., Gagnepain, J., Houseman, G., King, G.C.P., Papadimitriou, P., Soufleris, C., Virieux, J., 1982. Seismicity, normal faulting, and the geomorphological development of the Gulf of Corinth (Greece): the Corinth earthquakes of February and March 1981. Earth and Planetary Science Letters 57 (2), 377–397.
Knipe, R.J., Jones, G., Fischer, Q.J., 1998. Faulting, fault sealing and fluid flow in hydrocarbon reservoirs: an introduction. In: Jones, G., Fisher, Q.J., Knipe, R.J. (Eds.), Faulting, Fault Sealing and Fluid Flow in Hydrocarbon Reservoirs. Geological Society, London Special Publication, vol. 147, pp. vii–xxi.
Kokkalas, S., Koukouvelas, I.K., 2005. Fault-scarp degradation modeling in central Greece: the Kaparelli and Eliki faults (Gulf of Corinth) as a case study. Journal of Geodynamics 40 (2–3), 200–215.
Koukouvelas, I.K., Katsonopoulou, D., Soter, S., Paraskevas, X., 2005. Slip rates on the Helike Fault, Gulf of Corinth, Greece: new evidence from geoarchaeology. Terra Nova 17 (2), 158–164.
Labaume, P., Carrio-Schaffhauser, E., Gamond, J.-F., Renard, F., 2004. Deformation mechanisms and fluid-driven mass transfers in the recent fault zones of the Corinth Rift (Greece). Comptes Rendus Geosciences 336 (4–5), 375–383.
Lee, J.-J., Bruhn, R.L., 1996. Structural anisotropy of normal fault surfaces. Journal of Structural Geology 18 (8), 1043–1059.
Leeder, M.R., Collier, R.E.L., Abdul Aziz, L.H., Trout, M., Ferentinos, G., Papatheodorou, G., Lyberis, E., 2002. Tectono-sedimentary processes along an active marine/lacustrine half-graben margin: alkyonides Gulf, E. Gulf of Corinth, Greece. Basin Research 14 (1), 25–41.
Leeder, M.R., Mack, G.H., Brasier, A.T., Parrish, R.R., McIntosh, W.C., Andrews, J.E., Duermejier, C.E., 2008. Late-Pliocene timing of Corinth (Greece) rift margin fault migration. Eart and Planetary Science Letters 274, 132–141.
Leeder, M.R., McNeill, L.C., Collier, R.E.L., Portman, C., Rowe, P.J., Andrews, J.E., Gawthorpe, R.L., 2003. Corinth rift margin uplift: new evidence from Late Quaternary marine shorelines. Geophysical Research Letters 30 (12), 1611.
Lin, A., 1996. Injection veins of crushing-originated pseudotachylyte and fault gouge formed during seismic faulting. Engineering Geology 43, 213–224.
Lindanger, M., Gabrielsen, R.H., Braathen, A., 2007. Analysis of rock lenses in extensional faults. Norwegian Journal of Geology 87, 361–372.
Malartre, F., Ford, M., Williams, E.A., 2004. Preliminary biostratigraphy and 3D geometry of the Vouraikos Gilbert-type fan delta, Gulf of Corinth, Greece. Comptes Rendus Geosciences 336 (4–5), 269–280.
Means, W.D., 1987. A newly recognized type of slickenside striation. Journal of Structural Geology 9 (5–6), 585–590.
Micarelli, L., Benedicto, A., Wibberley, C.A.J., 2006a. Structural evolution and permeability of normal fault zones in highly porous carbonate rocks. Journal of Structural Geology 28 (7), 1214–1227.
Micarelli, L., Moretti, I., Daniel, J.M., 2003. Structural properties of rift-related normal faults: the case study of the Gulf of Corinth, Greece. Journal of Geodynamics 36 (1–2), 275–303.
Micarelli, L., Moretti, I., Jaubert, M., Moulouel, H., 2006b. Fracture analysis in the south-western Corinth rift (Greece) and implications on fault hydraulic behavior. Tectonophysics 426 (1–2), 31–59.
Moretti, I., Sakellariou, D., Lykousis, V., Micarelli, L., 2003. The Gulf of Corinth: an active half graben? Journal of Geodynamics 36 (1–2), 323–340.
Morewood, N.C., Roberts, G.P., 1999. Lateral propagation of the surface trace of the South Alkyonides normal fault segment, central Greece: its impact on models of fault growth and displacement–length relationships. Journal of Structural Geology 21 (6), 635–652.
Morewood, N.C., Roberts, G.P., 2001. Comparison of surface slip and focal mechanism slip data along normal faults: an example from the eastern Gulf of Corinth, Greece. Journal of Structural Geology 23 (2–3), 473–487.
Nøttveit, H., Tveranger, J., Espedal, M.S., Bastesen, E., Braathen, A., 2007. Structuring fault outcrop data for numerical modelling purposes. In: AAPG IECE, Athens.
Ori, G.G., 1989. Geologic history of the extensional basin of the Gulf of Corinth (?Miocene–Pleistocene), Greece. Geology 17, 918–921.
Peacock, D.C.P., 2002. Propagation, interaction and linkage in normal fault systems. Earth-Science Reviews 58 (1–2), 121–142.
Petit, J.P., 1987. Criteria for the sense of movement on fault surfaces in brittle rocks. Journal of Structural Geology 9 (5–6), 597–608.
Le-Pichon, X.L., Angelier, J., 1979. The Hellenic arc and trench system: a key to the neotectonic evolution of the eastern Mediterranean area. Tectonophysics 60, 1–42.
Poulimenos, G., 1991. Tectonic and Sedimentary Analysis of the Western Part of the Corinth Rift. University of Patras.
Riedel, W., 1929. Zur mechanic geologischer brucherscheinungnen. Zentral-blatt fur Mineralogie, Geologie und Paleontologie B, pp. 354–368.
Roberts, G., Stewart, I., 1994. Uplift, deformation and fluid involvement within an active normal fault zone in the Gulf of Corinth, Greece. Journal of the Geological Society of London 151, 531–541.
Roberts, G.P., Koukouvelas, I.K., 1996. Structural and seismological segmentation of the Gulf of Corinth fault system: implication for models of fault growth. Annali di Geophysica 39, 619–646.
Rohais, S., Eschard, R., Ford, M., Guillocheau, F., Moretti, I., 2007. Stratigraphic architecture of the Plio-Pleistocene infill of the Corinth Rift: implications for its structural evolution. Tectonophysics 440 (1–4), 5–28.
Rykkelid, E., Fossen, H., 2002. Layer rotation around vertical fault overlap zones: observations from seismic data, field examples, and physical experiments. Marine and Petroleum Geology 19 (2), 181–192.
Sammis, C.G., Osborne, R.H., Anderson, J.L., Banerdt, M., White, P., 1986. Self-similar cataclasis in the formation of fault gouge. Pure and Applied Geophysics 124 (1/2), 53–78.
Sibson, R.H., 1977. Fault rocks and fault mechanisms. Journal of the Geological Society of London 133, 191–213.
Solheim, M., 2002. Et strukturgeologisk feltstudium av roterte forkastingsblokker relatert til rampe-flate-rampe ekstensjonsforkastinger i Korint, Hellas, og på Lavransfeltet, midtnorsk kontinentalsokkel. Unpublished Strukturgeologi og Petroleumsgeologi thesis, Universitetet i Bergen.

Sorel, D., 2000. A Pleistocene and still-active detachment fault and the origin of the Corinth-Patras rift, Greece. Geology 28, 83–86.
Stewart, I.S., Hancock, P.L., 1991. Scales of structural heterogeneity within neotectonic normal fault zones in the Aegean region. Journal of Structural Geology 13 (2), 191–204.
Sverdrup, E., Skov, T., Solheim, M., Aarseth, E., Gabrielsen, R.H., 2001. The use of field data from the faulted margin of the Gulf of Corinth as input to the reservoir model for the Lavrans Field, Haltenbanken, Offshore Norway. In: Proceedings of the Ninth International Congress, Athens, September 2001. Bulletin of the Geological Society of Greece, vol. XXXIV/1, pp. 337–343.
Tarasewicz, J.P.T., Woodcock, N.H., Dickson, J.A., 2005. Carbonate dilation breccias: examples from the damage zone to the Dent Fault, northwest England. Geological Society of America 117 (5/6), 736–745.
Tchalenko, J.S., 1970. Similarities between shear zones of different magnitude. Geological Society of America Bulletin 81, 1625–1640.
Tveranger, J., Braathen, A., Skar, T., Skauge, A., 2005. Centre for integrated petroleum research – research activities with emphasis on fluid flow in fault zones. Norwegian Journal of Geology 85, 63–72.
Westaway, R., 2002. The Quaternary evolution of the Gulf of Corinth, central Greece: coupling between surface processes and flow in the lower continental crust. Tectonophysics 348 (4), 269–318.
Woodcock, N.H., Fisher, M., 1986. Strike-slip duplexes. Journal of Structural Geology 8 (7), 725–735.
Xypolias, P., Koukouvelas, I.K., 2001. Kinematic vorticity and strain rate patterns associated with ductile extrusion in the Chelmos Shear Zone (External Hellenides, Greece). Tectonophysics 338 (1), 59–77.
Yielding, G., Freeman, B., Needham, D.T., 1997. Quantitative fault seal prediction. American Association of Petroleum Geologists Bulletin 81, 897–917.
Zygouri, V., Verroios, S., Kokkalas, S., Xypolias, P., Koukouvelas, I.K., 2008. Scaling properties within the Gulf of Corinth, Greece; comparison between offshore and onshore active faults. Tectonophysics 453 (1–4), 193–210.